University of Alberta

Hydrogen induced hardening effects on alpha iron: a molecular dynamics study

by

Wenbo Xie

A thesis submitted to the Faculty of Graduate Studies and Research

in partial fulfillment of the requirements for the degree of

Master of Science

in

Materials Engineering

Department of Chemical & Materials Engineering

Fall 2011

Edmonton, Alberta

To my mother Yu Jiang, my father Shuzhi Xie, my sister Yaping Xie, my brother-in-law Shengyu Wang, my little niece Xi’na Wang

Abstract

Molecular dynamics simulations were performed to investigate the hydrogen interaction with edge dislocations during deformation in α-Fe. In particular, uniaxial tensile tests at different lattice hydrogen concentration were conducted in a single crystal iron with high density of edge dislocations introduced by plastic deformation. During system relaxation, hydrogen atoms have tendency to diffuse and stay around dislocation line - a well-known hydrogen trap-site in α-Fe. Our simulations show that the yield strength of the bcc iron is very sensitive to the presence of hydrogen within edge dislocations, i.e., it increases as hydrogen concentration increasing. After yielding, the hydrogen atom is de-associated with the moving dislocations, suggesting that the yield strength enhancement is due to the hydrogen pinning effect. This direct observation of hydrogen hardening effects confirms the model suggested by Matsui etc. Additional simulations also indicate hydrogen interaction with edge dislocations is sensitive to temperature as well as vacancies around dislocation cores.

Acknowledgements

It is a pleasure to thank many people who helped me make this thesis possible. I have been indebted to my supervisors Hao Zhang and Weixing Chen who made their support available in a numerous ways. Their patience, kindness, guidance have carried me through my entire study. Particularly their relentless enthusiasm towards perfection and deep perception regarding scientific research has become a constant source of my strength and inspiration for my academic exploration and future career. I believe they are the best mentors and role models I could ever ask for along the road of my academic pursuit.

I am grateful that my families have always put up with the fact that I have been so far away from home ever since I was 14 and supported me under no condition especially my sister who backed me up in each every way she could have possibly done.

I also want to extend my gratitude to people who helped me grow and enlightened me through the years. I learnt perseverance from Yang Chen, loyalty from Jingbo Jin, generosity from Jirong An.

My life would have been incomplete without their companion and encouragement all the way along.

Help from my student colleagues and dear friends, Guilin Wang, Jing Wang, Peng Huang, Yang Pan, Su Tian, Huiran Wang, Lei Wang, Kaiwen Liu, Jie Zhang, Arina Marchenko and Dr. Fengping Hu, Dr. Yongwang Kang, Dr. Xiaoyang Liu were also greatly acknowledged. It is the help and companionship of them that made my life more colorful and meaningful.

Table of Contents

Abstract 3

Acknowledgements 4

1 Introduction 1

1.1 Hydrogen embrittlement 1

1.2 Main hydrogen embrittlement mechanism 2

1.2.1 Hydride formation and cleavage mechanism 3

1.2.2 Hydrogen enhanced local plasticity (HELP) 4

1.2.3 Hydrogen enhanced decohesion theories (HEDE) 5

1.3 Computer simulation on hydrogen embrittlement in α iron – hydrogen induced softening or hardening 6

1.3.1 Hydrogen - vacancy interactions 7

1.3.2 Hydrogen - grain boundary interactions 9

1.3.3 Hydrogen crack tip interactions 11

1.3.4 Hydrogen dislocation interactions 13

1.4 Objective of this thesis 20

2 Simulation Methodology 20

2.1 Fundamental principles of MD simulation 23

2.2 Potential 25

2.2.1 Pair potential – Lennard –Jones Potential 25

2.2.2 Many body potential – Embedded Atom Method Potential…….....….27
2.3 Integration Algorithm 28
2.3.1 Verlet Algorithm.....29
2.3.2 Velocity Verlet Algorithm 31
2.4 Temperature control.....32
2.4.1 Stochastic methods 33
2.4.2 Extended system method 33
2.4.3 Constraint methods 35
2.5 Pressure control.....36
2.5.1 Extended system methods.....36
2.5.2 Changing box-shape 37
2.6 Periodic boundary condition 38
2.7 Pressure calculation 39
2.8 Simulation model set up.....41
3 Hydrogen hardening mechanism.....47
3.1 Hydrogen diffusion in heavily deformed iron crystal48
3.2 Dislocation motion and hydrogen pinning during deformation….....51
3.3 Effect of hydrogen concentration on yield strength ..57
3.4 Temperature dependence of pinning effect 59

3.5 Influence of vacancies around dislocation core on yielding……. 61
4 Conclusion and future work 62
4.1 Conclusion 62
4.1.1 Hydrogen binding to crystal defects 63
4.1.2 Hydrogen induced hardening effect on yield stress…….. 63
4.1.3 Hydrogen pinning effect on edge dislocations.....63
4.1.4 Temperature effect on hydrogen pinning 64
4.1.5 Effect of vacancies around dislocation core on yielding……. 64
4.2 Limitation of current studies 64
4.3 Suggested the future work.....65
4.3.1 Crystallographic orientation & Dislocation 65
4.3.2 Screw dislocation & temperature.....65
4.3.3 Different microstructure 66

Table of Figure

Fig. 2.1 Schematic representation of MD simulation 24

Fig. 2.2 Stress tensors in three dimentions. 41

Fig. 2.3 Perfect 3D body-centered-cubic model composed by iron atoms colored in blue.....42

Fig. 2.4 Stress strain curve from initial tensile simulation.43

Fig. 2.5 Three dimension hydrogen free model filled with edge dislocations colored by pressure.....44

Fig. 2.6 2D Atomic stress (pressure) distribution of simulation cell without Hydrogen.....45

Fig. 2.7 Simulation process schematic.....47

Fig. 3.1 Hydrogen concentration profile along Z-direction at three different times 49

Fig. 3.2 2D hydrogen distribution diagram at the begin of the simulation corresponding to t = 0 ps in Fig. 3.1.. 49

Fig. 3.3 2D hydrogen distribution diagram corresponding to t = 500 ps in Fig. 3.1 50

Fig. 3.4 2D hydrogen distribution diagram corresponding to t = 3000 ps in Fig. 3.1 50

Fig. 3.5 Atomic configuration of the enlarged area in Fig.2.6…….. 52

Fig. 3.6 (a) Atomic configuration of the same enlarged area in Fig.2.6 (a) in the case of hydrogen free at ε= 0.2% (after yielding)…….....53

Fig. 3.6. (b) Atomic configuration of the partial simulation cell (the same enlarged area in Fig.2.6 (a)) in the case of 10 hydrogen at ε = 0.2% (before yielding). 53

Fig. 3.6. (c) Atomic configuration of partial simulation cell (the same enlarged area in Fig.2.6 (a))in the case of 10 hydrogen at ε=0.3% (after yielding). 54

Fig. 3.7 Yield strength as function of effective hydrogen concentration in dislocation. A typical stress strain curve is shown in the inset…….....59

Fig. 3.8 Yield strength as a function of temperature in the cases of hydrogen free and 10 hydrogen atoms. 61

1 Introduction

Hydrogen embrittlement is a severe phenomenon that affects the properties of materials greatly in reality. The deteriorating effects due to HE vary in a great range. This thesis study focuses on hydrogen effects on deformation behavior of a single crystal α iron with edge dislocations using molecular dynamics (MD) simulation method.

This thesis is organized as follows: chapter 1 includes a brief introduction of HE, its mechanism proposed so far which lays out the rationale why we are interested in hydrogen effect on the deformation behavior of α iron and related work to-date followed that to introduce the foundation our work is based on. In the next chapter, we describe the MD methodology in general and the specific details of our simulation model setup. In chapter 3, we present the simulation results on hydrogen-induced hardening due to the interaction between hydrogen and edge dislocations and also show how hydrogen concentration, temperature and vacancies around dislocation structure influence the hardening effect. In the last chapter of this paper, we draw conclusions based upon our observations and point out the limitations of current studies, then, point out the future work.

1.1 Hydrogen embrittlement

Hydrogen embrittlement (HE) was first documented in 1875 by Johnson[1]. It is a phenomenon that hydrogen solutes which were resulted from processing and exposure to environmental working

conditions penetrated into materials and caused deleterious effects on mechanical properties of metals. Reduction of ductility [2,3], detrimental impact on fatigue strength[4], impairment of fracture toughness[5], change of fracture mode and promotion on environmentally assisted cracking such as stress corrosion cracking [6] were extensively observed in the past. HE has been widely studied during the last five decades [6-14] and the significance of understanding HE mechanism has escalated as the promising future of "hydrogen economy" comes closer to the reality and HE related failures contributed to great economic loss and many catastrophic failures, particularly in oil & gas industry [6,13]. Although some studies implied that hydrogen might work against HE, leading to some beneficial effects[15], the majority of findings so far suggested that HE would degrade the mechanical properties of commercial steels[16]. Despite HE is found in almost all metals, our study focuses on α-iron (α-Fe) which is the most common element on the earth and the main component of commercial steels that have been widely used in the world.

1.2 Main hydrogen embrittlement mechanism

Based upon the assumption that HE is closely related to the interaction between hydrogen and dislocation motion[17,18] and experimental observations, different mechanisms have been proposed, three of which have gained wide supports. They are stress induced hydride formation and cleavage [19], hydrogen enhanced decohesion

theories (HEDE) [20], and hydrogen enhanced local plasticity (HELP) [17]. Concise explanations of the mechanisms are listed below.

1.2.1 Hydride formation and cleavage mechanism

Hydride formation and cleavage mechanism was originated from the discovery of hydrogen induced delayed cracking in steels which was discussed by Troiano and his coworkers who suggested that the process is a result of long range diffusion of hydrogen into a crack tip region under the local stress gradient[7]. Theoretical work relating to fracture mechanics has been performed on diffusion of point defects to crack tips under stress gradient[21]. Based on that, Vanleeuwen has built a quantitative model and concluded that a critical hydrogen concentration of hydrogen in solution at the crack tip is required to initiate the decohesion[22]. Arguments on whether hydrogen in solution or hydride caused HE have been validated through experiments. It is suggested that embrittlement effects could be produced either by hydride precipitation[19] or hydrogen in solution[23] depending on the specific scenarios where synergies of different metals, temperature and stress level etc. exist. Whereas, stress induced hydride formation was found frequently even in the region where temperature is above solvus[19,24]. Sufficient findings[25] supported hydride formation and cleavage mechanism to be one of the main three HE mechanisms. But it is only operative with hydride forming systems such as niobium [26], titanium [27] and zirconium[28] etc. Studies so far have shown HE occurs by hydride formation at stress

concentrators such as crack tips followed by cleavage of the brittle hydride. However, the process is not continuous as the crack propagates through hydride and stops while reaching the matrix. New hydride formation is either a auto-catalytical process[27] or a result of external loading, and then cleavage restarts[19]. More fundamental studies concluded hydride formation is a result of enhanced hydrogen concentration in the area of tensile stress[29] where the potential of hydride comparing to the solid solution was decreased[30]. The synergy of brittle hydride[31] , hydrogen concentration and stress field especially at crack tips have contributed to materials degradation.

In the systems that do not form hydrides, hydrogen enhanced local plasticity (HELP) and hydrogen enhanced decohesion theories mechanism (HEDE) come in effect.

1.2.2 Hydrogen enhanced local plasticity (HELP)

Studies on hydrogen effect on macroscopic flow stress yielded contradictory results, i.e., both flow stress increase (hardening)[32-37] and decrease (softening)[32-34,38] in metals have been observed. HELP was a main theory used to explain macroscopic flow stress decrease (softening). HELP mechanism states hydrogen presence increases local dislocation mobility. The reason behind that has been explained by several theories, for instant, Matsui and Moriya proposed decrease of Peierls-Nabarro barrier by hydrogen dislocation interaction[32,33], and the finding of Sofronis and Birnbaum suggests that it is the reduced effectiveness of solute pinning effect to dislocation motion due to

clustering of solute atoms and the decreased interactions between dislocations and other elastic centers as a result of hydrogen[39] that lead to enhanced dislocation mobility. The latter is commonly known as hydrogen shielding mechanism. In hydrogen shielding mechanism, hydrogen around dislocations shields interactions between dislocations and dislocation–solute. Thus, the interaction energies were reduced and dislocations became more mobile which was observed in experiments[40,41].

HELP mechanism has been observed in almost all metallic systems such as face-centered cubic (FCC)[42], body-centered cubic (BCC)[43] system, hexagonal close packed (HCP)[27] system and alloys[44].

1.2.3 Hydrogen enhanced decohesion theories (HEDE)

Hydrogen enhanced decohesion mechanism was first described in 1941 by Zapffe and Sims[45]. It is based on the postulate that hydrogen decreases the cohesive energy between atoms and promotes cleavages originally proposed by Steigerwald[7] et al. and enriched by Oriani and Josephic[9] who also extended the mechanism to interfacial fracture such as the reduction of cohesive strength of carbide –matrix interface[46]. For instance, it was shown the presence of hydrogen increased the population of microvoids in AISI 1045 steel and the failure mechanism is hydrogen enhanced decohesion at the cementite-ferrite interface[47]. The focus of this mechanism has been varied from the decohesion interface to hydrogen concentration. The experiments from Teter el al. had proposed a critical hydrogen concentration which

has to be reached before the reduction of cohesion of phase interface occurred in β-titanium[48].

Each mechanism so far has been supported through experimental observation. Unfortunately, a complete understanding of hydrogen embrittlement is still lacking owning to the complexity of microstructure of metallic systems and the difficulty of direct observation of hydrogen interaction with dislocations mainly because of small size, high diffusivity, and low solubility of hydrogen in metals [49] and the limits of current experimental technologies.

1.3 Computer simulation on hydrogen embrittlement in α iron – hydrogen induced softening or hardening

As an alternative to experiment, numerical calculation / simulations serve an important role in understanding the proposed HE theory. It is becoming increasingly popular with the advance of computer science and efficient calculation algorithm. Computer simulation provides researchers a microscopic resolution that cannot be reached by experiments at current technology level. In this chapter, both experimental work and simulation studies on α iron would be reviewed with respect to hydrogen induced hardening and softening. However, the main focus will be given to simulation studies.

The computer simulation method varies. For instance, quantum MD using first principle can only simulate a very small system of hundreds or less atoms, while classic MD (based on Newton's second

law instead of quantum theories in quantum MD) could deal with relatively big system. Simulation methods such as atom superposition and electron delocalization molecular orbital cluster (ASED-MO) method; Monte Carlo simulation method, ab initio MD simulation, molecular static (MS) simulation are widely employed. MD simulation used in this thesis study refers to classical MD.

HE is a combination of stress, hydrogen and environmental factors. Thus, the simulation study of HE is still revolved around these 3 factors. It is believed that HE induced deterioration of materials properties could be attributed to the interactions among hydrogen and the lattice imperfections, i.e. vacancies, grain boundary, crack tip, and dislocations etc. The trapping effects of lattice defects towards hydrogen have been established long time ago. In the following, studies of hydrogen interactions with them were reviewed.

1.3.1 Hydrogen - vacancy interactions

Hydrogen – vacancies interaction had drawn quite a lot of attention through the years. Itsumi and Ellis had studied the electronic structure of α iron clusters involving a vacancy and compared the results of models with and without interstitial hydrogen using self-consistent discrete variational method within the local density functional formalism. It is found that first of all interstitial hydrogen greatly reduces the local Fe-Fe bond within a small distance of 0.3 nm. Secondly, in a perfect bcc Fe lattice, interstitial hydrogen is subjected to repulsive force and volume expansion is observed. Thirdly, with the

presence of vacancy, hydrogen prefers a position shifting from the octahedral site toward the vacancy. The main effect of the vacancy is to increase Fe-H bond at the expense of Fe–Fe bond, which supported decohesion mechanism of Fe –Fe bond in HE[50].

Juan and Hoffmann studied the electronic structure of bulk bcc iron and confirmed the conclusion that vacancy introduction leads to Fe – H bond formation which in turn reduces Fe-Fe bond (as much as 30% reduction was observed) using band structure calculation and ASED-MO cluster method. In addition, a comparison was drawn on hydrogen adsorption at the Fe (110) surface with hydrogen near bulk Fe with a vacancy. Apparently detrimental effect of hydrogen is more severe in a vacancy than on the surface[51]. Studies of Irigoyen et al. concluded hydrogen residing in a vacancy decreases the total energy in α iron and hydrogen tends to form H-H pairs within the vacancy, thus very hard to diffuse out due to the high energy barrier[52].

Pronsato et al. used density functional theory to study an iron cluster of 12 atoms with a vacancy. The main feature of hydrogen – iron interaction is in line with previous studies on larger clusters. Hydrogen atoms do not bond with each other but bond with closest Fe atoms, weakening the existing Fe-Fe bonds[53]. Tetayama et al. investigated the stability of hydrogen – vacancy complexes from a point of view of energetic in α iron and concluded the binding preference of hydrogen in bcc iron by means of *ab initio* supercell calculation based on density functional theory. They also presented

the theoretical support for hydrogen enhanced vacancy formation suggested by experiments[54].

These simulation studies had coincided with the experimental studies that strongly suggested hydrogen accelerated lattice defect formation under strain condition and contributed to properties degradation[55].

1.3.2 Hydrogen - grain boundary interactions

Other than vacancies, grain boundary is subjected to great interests too as the network of grain boundary forms microstructure of materials that determine many aspects of materials mechanical properties.

Farkas et al. had correlated the cracking to loading value and the impurity. They studied fracture behavior of a pure sigma 5 symmetric tilt grain boundary in α iron at low temperatures and found that the crack propagation mode (intergranular or intragranular /transgranular cracking) is sensitive to the loading value. For loadings just above the Griffith value, the crack propagates along the boundary for a distance of about 5 nm and then deflects toward the grains. When the boundary is loaded way above the Griffith value, the crack propagates intragranularly. The effects of impurities on crack propagation along the grain boundary were studied and the presence of hydrogen impurities resulted in a significant decrease in cohesive energy of bonding at grain boundary (embrittling the grain boundary),

which made cracking propagates along the grain boundary instead of deflecting into the grain. Molecular statics simulation was used in this study[56].

Itsumi and Ellis calculated on electronic structure of two grain boundaries, sigma 3(111) and 3(110) with the presence of hydrogen using first principle method and confirmed that hydrogen occupation at grain boundaries would expand the volume of grain boundaries. Reduction of Fe – Fe bond due to hydrogen presence at grain boundaries was also discovered[57]. Above studies supported the experimental findings of hydrogen induced intergranular fracture of steels.

Other than findings in fracture phenomena, there were studies focusing on fundamentals such as hydrogen diffusion and trapping in defects. For instance, Liu et al. studied hydrogen diffusion among sigma 5[100]/(013) symmetrical tilt grain boundary, free surface(001) and the bulk materials in α iron in a temperature range of 400 and 700 K, as predicted grain boundary has the strongest trapping ability, then free surface and the bulk materials. The inclination effect of grain boundary on hydrogen diffusion, i.e., hydrogen diffusivity in a series of sigma 5[100] tilt grain boundary was discussed using MD simulation. Two local maxima of the activation energy for hydrogen diffusion were found at two symmetric tilt grain boundaries. Additional calculation of boundary excess volume yielded two local minima at the same symmetric grain boundaries which lead to a suggestion that excess gain boundary volume and stress assisted

hydrogen diffusion at grain boundary. They also studied hydrostatic pressure on diffusion and concluded that tensile stress tends to promote hydrogen diffusion in lattice into grain boundary or surface traps while compressive stress leads to a decrease in diffusivity and a slower rate of filling to those traps[58].

1.3.3 Hydrogen crack tip interactions

To study the possible mechanism of hydrogen induced cracking or fracture model change, crack tip scenario had gained sufficient attention.

Markworth and Hirth pioneered crack tip study in iron by MD with the pair potentials using a simple designed two dimensional (2D) model to characterize crack extension by kink motions. They found the strain dependence of kink barriers against crack extension and healing as well as decohesion effect by foreign atoms[59,60]. Mullins studied the behavior of a crack tip inside the single crystal of α iron with hydrogen atoms using MD. A Morse potential of a longer ranged nature was used. It is found blunting of the crack tip by spontaneous dislocation nucleation occurs under most situations. The presence of hydrogen inhibits the blunting and then enhances brittle fracture. The necessity of improving accuracy of potential was mentioned [61].

Decelis et al. studied three dimensional (3D) crack tip processes in α iron. They simulated crack tip processes of α iron and copper via molecular dynamics approach using Johnson and Morse potentials.

Alpha iron is found to be inherently brittle, and failed by cleavage along a cube plane when the stress intensity factor reaches the critical Griffith value and copper is inherently ductile[62].

Hu et al. studied a 3D crack tip model in a single crystal of α iron composed of a {100} plane using Morse pair potential under uniaxial tension along <100> direction at 293 K by means of MD simulation. They considered HE as a three-step process where it starts from cavity nucleation, then cavity linkage, finally fracture. He found cavity nucleation occurs on the (100) plane in the notched area with more than 3 hydrogen atoms and it is independent of hydrogen content. The deformation step of cavity linkage and fracture decreases logarithmically with increasing hydrogen content[63].

Telitchev and Vinogradov combined molecular static and MD methods using modified Morse pair potential to study a 3D crystal structure with model I crack in α iron by performing nano-scale tensile tests and the stress strain curves were obtained for the deformation process. They suggested that hydrogen near crack tip lead to severe distortion of α iron structure and a loss of strength. The degradation of strength is sensitive to the hydrogen presence but did not increase proportionally with the increasing hydrogen concentration[64]. Taketomi et al. investigated the hydrogen effect on dislocation emission around a model II crack tip in α iron by means of molecular static simulation using EAM potentials. He claimed that hydrogen atoms located a few angstroms away from crack tips enhanced dislocation emission around a {112}<111> edge dislocation

due to the reduction in the critical stress intensity factor and he attributed this enhanced emission to the reduction in stacking fault energy which is supportive to HELP mechanism[65].

Matsumoto and his colleagues conducted MS simulation and concluded that hydrogen atoms on a slip plane promote the separation of the slip plane due to the decrease in its surface energy as a result of hydrogen presence. They also studied model I crack propagation using MD simulation. Hydrogen tends to be trapped in dislocation cores and along slip planes in the vicinity of a dislocation core. The hydrogen atoms in dislocation core reduce the energy barrier for dislocation motion and thus increase dislocation mobility. They combined HEDE and HELP to explain HE since HELP is related to dislocation motion which is prior to fracture and HEDE is used to explain fracture, i.e., crack propagation[66].

Most hydrogen crack tip interactions studies so far agree with the HEDE mechanism. Studies frequently included dislocations around crack tips as dislocations are the key element in plastic deformation. Dislocation-hydrogen interactions will be introduced below.

1.3.4 Hydrogen dislocation interactions

Hydrogen dislocation interactions have been extensively studied due to the significance of dislocation motion to deformation behavior of metals. We only focus on α iron here.

Hydrogen binding to dislocations has been proven for both edge and screw dislocations such as the work conducted by Taketomi et al. [67]in which a molecular statics analysis was performed to study hydrogen trap energy around {112} <111> edge dislocation in α iron. They concluded that hydrogen trap energy is sensitive to both hydrostatic stress and shear stress, indicating strong trap sites are across a wide range on slip plane around dislocation core. Matsumoto et al. [68] estimated the distributions of hydrogen trap energy around the {112} <111> edge dislocation and {112} <111> screw dislocation for α iron and aluminum using first principles calculations. Hydrogen dislocation interaction is stronger in α iron than that in aluminum. It is found that strong trap sites are in the vicinity of the edge dislocation and the screw dislocation in α iron.

Here we look at hydrogen dislocation interactions from a perspective of how hydrogen affects dislocation mobility and its linkage to macroscopic property of materials, especially hardening or softening in terms of yield stress.

A large amount of work suggested that hydrogen could have contradictory effects on dislocation motions: either enhancing dislocation mobility (basis for HELP mechanism) [69] or dragging (or pinning) dislocation motion[32,70], which microscopically leads to hydrogen induced softening and hardening, respectively [49,71,72]. Previous studies on hydrogen-induced softening/hardening have been mainly focused on steels[35,70,71,73].

Studies had suggested that the change of flow stress with hydrogenation depended on many factors such as pre-strain, grain – size[74]. Asano and Otsuka observed that commercial mild steels being deformed initially without hydrogen raises the flow stress if the specimen wire has a radius greater than 0.63 mm, but lowers the stress of specimens of smaller radius at ambient temperature, thus, conclude specimen-size as a factor affecting flow stress [75].

Oriani and Josephic examined hydrogen effect on the plastic deformation of pearlitic and spheroidized 1045 steels. They found hydrogen in dissolved state invariably hardens the 1045 steels. But the hydrogen at a very high input activity increased the population of micro-voids and caused a softening effect[35].

Apparently based on the above studies, there are quite a few factors such as grain size, pre-strain, size of the specimen, hydrogen activity etc. that influence the hydrogen effects on steels which made the effect more complicated than it already was. To study this multi-causal phenomenon, the scientific method is to isolate each factor and investigate each individual effect, thus, works performed in high purity iron were used to minimize the alloy effects. Interestingly, hydrogen-induced hardening is more likely to be observed in pure iron systems[72,75-77]. For instance, Asano et al. had re-examined the effect of hydrogen on the flow stress of iron (as opposed to their work on steels) using cathodic charging method and found the flow stress increased very rapidly after the start of cathodic charging hydrogen

for the pure iron. He also inferred that this hardening effect would be applicable to all bcc ferritic alloys[78].

The contradictory effects of macroscopical hardening /softening induced by hydrogen were believed to be related to hydrogen – dislocation interactions, i.e. whether hydrogen could increase the mobility of dislocations i.e. HELP mechanism, or decrease the mobility, i.e. hydrogen induced pinning or dragging effect.

Systematic studies by Matsui et al. [32] and Kimura et al. [77] had shown both hydrogen-induced hardening and softening in high purity iron at low temperatures. Their experimental results suggested that hydrogen trapped in screw dislocations increases dislocation mobility from 200 K to 300 K, which resulted in softening, while hydrogen hinders the motion of edge dislocations as well as kinks on screw dislocations below 200K, which led to hardening. They attributed hydrogen-induced softening to the hydrogen effects on kink pair nucleation and kink mobility of screw dislocations and indicated the possibility of hydrogen pinning effect with edge dislocation.

Lan et al. [79] confirmed the similar mechanism by conducting a tensile experiment on α iron of different dislocation structure, i.e., screw dislocations and non-screw dislocations and concluded hydrogen effect on the flow stress depended on the purity of specimens and also suggested hydrogen can both enhance the rate of kink pair formation and act as barriers against the side ward motion of kinks at and below ambient temperature. For the effect of hardening or softening on screw dislocation, it depends on what process is

dominant. They also found the hampering to motion of edge dislocations by hydrogen – carbon atoms.

A different opinion addressing hydrogen induced softening was suggested by Zhang et al. who claimed that hydrogen atmosphere (strain field) enriched around the crack tip introduced an additional stress which helped the external stress to move dislocations against its resistance. As a result, the yield stress is decreased markedly[80,81].

Comparing to experimental studies on hydrogen dislocation interactions, simulation work associated with hydrogen induced softening and hardening is very limited.

For study of hydrogen induced softening, Wen et al.[82] confirmed the correlation between hydrogen induced softening and screw dislocations by means of performing atomistic simulations using nudged elastic band method to estimate the hydrogen effect on the activation energy for kink-pair nucleation near a screw dislocation and confirmed that hydrogen-induced softening/hardening is related to the transition of hydrogen to its stronger/weaker binding sites, i.e., when a kink pair nucleates at hydrogen, the activation energy is decreased by the transition of hydrogen to a stronger binding site, inducing softening. When a kink pair nucleates at hydrogen, the activation energy is increased by the transition of hydrogen to a weaker binding site, inducing hardening.

Juan et al. [83] studied H-Fe interaction in a system including an $a/2[1\bar{1}1]$ dislocation by means of ASED-MO method and compared

with previous results for an *a*[010] edge dislocation. Despite the difference in core dislocation structure, they both behave in a very similar way such that hydrogen stabilizes in the dislocation void and the Fe-H interaction is favored in dislocation area over H-H bonding. In both types of dislocations, hydrogen diminished Fe-Fe bond strength of the nearest neighbors around 30-40% of its original value. Increased dislocation mobility was also observed with hydrogen presence. Their findings would support hydrogen induced softening either from a decohesion point of view, in which Fe-Fe bond was reduced thus, yield stress could be lower, or from a HELP mechanism whereby dislocation mobility was increased by hydrogen.

For the study of hydrogen induced hardening, Weber et al. [84] proved the linkage of hydrogen to the reduction in ductility and crack resistance in steel 15MnNi6-3 experimentally and numerically for α iron at the room temperature and higher. Their simulations showed hydrogen along the edge dislocation line at 0K and at room temperature can reduce the dislocation movement. Further simulations concluded that the reduction in materials ductility is due to the weakening of atomic bindings. Despite, it did not explicitly refer to hardening or softening, it suggested hydrogen impedes the movement of dislocations.

Nedelcu et al. [85]studied hydrogen atoms interaction with edge dislocation in α iron below ambient temperature and concluded the importance of the initial positions of hydrogen atoms. If hydrogen initially occupied in the vacancy position, motion of edge dislocation

would be blocked and hardening would occur macroscopically as the internal stress could not be released, while hydrogen occupied in interstitial sites might help dislocation motion and support HELP mechanism.

Although previous studies have established a connection between hydrogen-induced hardening/softening to the interaction of hydrogen with dislocations at low temperature domain, many supported that hydrogen – screw dislocation interaction is the key to softening phenomenon. The relationship between hardening/softening and the interaction of hydrogen with edge dislocations is still unclear. In addition, despite that screw dislocation predominates the plastic deformation mechanisms of BCC metals at a low temperature range [86-91], current thesis focuses on the interaction between hydrogen and edge dislocations which is very crucial to the discussion of initial deformation behavior of alpha iron where edge dislocations move much faster than screw dislocations[84,92] and the preponderance of edge dislocations in high purity iron has been previously established[93]. Other studies have shown the existence of areas mainly filled with edge dislocations especially around the plastic zone close to a crack tip [94] which significantly affected the materials deformation and cracking mechanisms. That sums up the significance of the interaction between hydrogen and edge dislocations in a heavily deformed single crystal iron.

1.4 Objective of this thesis

A general review of three widely supported HE mechanisms had yielded the complex yet contradictory findings of HE, however, the consensus was reached that the complicated nature of HE is attributed to hydrogen – dislocations interactions. Up-to-date studies on hydrogen effects on deformation behavior of α iron and steels, specifically hydrogen induced change in dislocation mobility which relates to hardening and softening macroscopic behavior had indicated the insufficiency of research in the area of hydrogen – edge dislocation interaction as compared to hydrogen – screw dislocations interaction which explained well hydrogen induced softening effect at low temperature range. In addition, direct observation of hydrogen – edge dislocations effect in hardening or softening was lacking. The objective of this thesis is to explore the effect induced (hardening or softening) by hydrogen - edge dislocations interaction in a heavily deformed single crystal α iron under tensile deformation.

2 Simulation Methodology

Molecular dynamics simulation is the modern realization of an old fashioned idea in science to interpret nature in a deterministic mechanical way. Namely, the behavior of a system can be computed given a set of initial conditions and atomic interactions [95].

It is a technique used to compute the equilibrium and transport properties of a classical many body system which follows Newton's

motion of equation[96]. Note that for systems in non-equilibrium, MD has to be adapted in order to sample the non-equilibrium ensembles and this non-equilibrium molecular dynamics is more effective in calculation of transport propertied[97] .

Molecular dynamics originated from the statistical methods of studying large numbers of particles by Maxwell and Boltzmann [98]. MD simulation method was first introduced by Alder and Wainwright in 1950's to study the dynamics of an assembly of hard spheres[99]. Real materials MD simulation was conducted by Gibson et al. in analyzing copper's radiation damage[100]. Rahman was the first to employ realistic potential in simulating liquid argon[101] .

This method could compute thermodynamic, structural and kinetic properties, e.g., yield strength, interfacial energy, diffusivity and etc. It also allows scientists to study the motion of individual atoms, which is not possible in laboratory experiments. It has been widely used in the study of materials science. MD simulation is more effective and easy to control computational experiment's conditions such as temperature and pressure when material's size is down to nanometer scale.

Despite of all advantages brought by MD, one of the major limitations is its discrepancy in spatial and temporal resolution with real experiments. Nevertheless, the application of periodic boundary conditions provides an approach to extend simulation system from a finite small volume to infinitely large. For truly periodic systems, e.g.,

periodic single crystal, only small simulation system is needed. However, when we deal with systems with defects or calculate kinetic and dynamical quantities, large simulation system is needed. The largest simulation system may contain atoms on the order of 10^9. Of course, computational expense would be extremely high in that case and still smaller than the real material scale of 10^{23}. Due to the widespread interest in nano-scale materials, spatial resolution of real experiment and that of simulation becomes closer. The other discrepancy is temporal resolution inconsistency which is limited by Debye frequency as the time resolution has be to smaller than the Debye frequency in order to capture the trajectory of all atoms in the simulation system. In addition, it usually takes more than days or even months to finish simulations for a system composed of hundreds of thousands of atoms through state-of-art CPUs. Depending the size and complexity of the simulation system as well as the specific settings, the simulation time varied. Nevertheless, simulations are commonly carried out on the order of nanoseconds. Apparently the total length of simulation could certainly be extended with the advance of computational algorithm and hardware upgrade in the future.

In the following chapter, fundamental principles of the MD simulation method, temperature control, pressure control, simulation configuration, employed algorithm and the choice of inter-atomic potentials will be discussed.

2.1 Fundamental principles of MD simulation

The key notion in molecular dynamics simulation is motion, which is based on Newton's second law of motion:

$$\overrightarrow{F_i} = m_i \overrightarrow{a_i} \qquad [2.1.1]$$

where $\overrightarrow{F_i}$, m_i and $\overrightarrow{a_i}$ are the force, mass and acceleration of atom i , respectively. As the force on each atom is determined from potential, acceleration of each atom would be calculated if the potential is known. Hence, integration of the equation of each atom yields the trajectories, i.e. positions, velocities and accelerations of each atom as a function of time. Thus, the average values of system properties could be determined based on statistical mechanics. The inputs are potential, initial positions and velocities of each atom in the system for MD simulation.

To calculate the force of each atom, the relationship between inter-atomic potential and force is as follows:

$$\overrightarrow{F_i} = -\nabla V(r_i) \qquad [2.1.2]$$

where V represents inter-atomic potential , r_i represents the i atom's position. Combining two equations yields:

$$-\nabla V(r_i) = m_i\left(\frac{\partial^2 r_{ix}}{\partial t^2}, \frac{\partial^2 r_{iy}}{\partial t^2}, \frac{\partial^2 r_{iz}}{\partial t^2}\right) \qquad [2.1.3]$$

The equation [2.1.3] has shown the initial inputs needed to conduct a MD simulation. Each of them would affect the trajectories of simulations especially the interatomic potential V as the accuracy of

V would directly determine the reliability of simulation results in terms of how close the dynamics of atoms is to the reality. More information on potentials will be introduced in the next chapter.

To better understand the process of MD simulation, the following schematic graph is used.

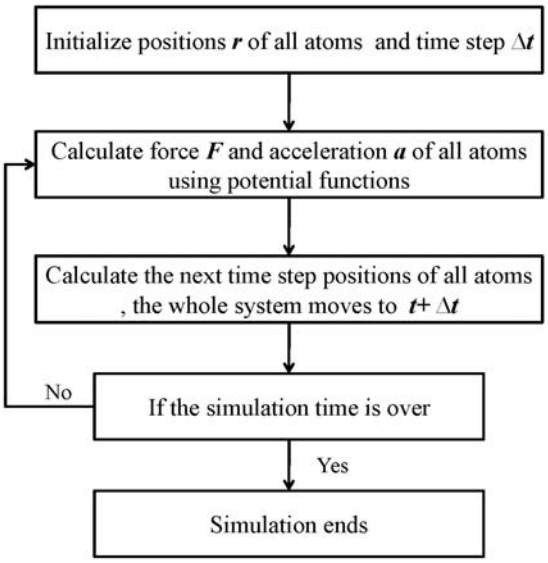

Fig. 2.1 Schematic representation of MD simulation

The simulation proceeds repetitively by alternatively calculating forces and solving the equations of motion based on the accelerations obtained from the new forces. In practice, almost all MD codes not only have to integrate the equation of motion but also involve additional steps to realize temperature, pressure control, data analysis and output. These are related to the ensemble chosen in MD simulation; also vary with the targets of simulation as well as the hardware support. As pointed, there are a few key components worth

elaborating such as potential, integration algorithm (solving equation of motion), temperature control, pressure control, in which would be introduced in the following chapters.

2.2 Potential

Potential energy function is used to model the basic interactions among atoms or molecules. There are basically two types of potentials used in general sense. The first one came from solving Schrodinger equation for the electrons, of course, during which approximation has to be made. One of these approximation methods is to use density function theory. This approach in which nuclei follows motion of classic mechanics while potentials were evaluated through solving Schrodinger equation of electronics is known as ab inito calculation. Another type of potentials being parameterized analytical potential employed drastic simplification. It only depends on the position of nuclei and usually obtained through fitting experimentally measured data. It is also known as empirical potentials. This method is so called classical molecular dynamics which is used in current thesis study. There are mainly two types of empirical potentials in modeling solids as explained below: pair potential and many-body potential[102].

2.2.1 Pair potential – Lennard –Jones Potential

The pair potential treats the overall energy of the system as a sum of atomic pair wise interactions while many-body potential

considers energy contribution from the third and more atoms in addition to the pair wise interaction.

Lennard-Jones or otherwise known as 6-12 potential is a classical pair potential shown as

$$V = 4\varepsilon((\frac{\sigma}{r})^{12} - (\frac{\sigma}{r})^{6})$$

Lennard-Jones potential contains two terms, repulsion part $(\frac{\sigma}{r})^{12}$, dominating at short distance when atoms or molecules are close and attraction part $(\frac{\sigma}{r})^{6}$, dominating at a large distance. Here, ε is the depth of the energy well and σ is the interparticle spacing when the pairwise potential equals zero. These parameters σ and ε are chosen to fit the physical properties of the material.

Lennard-Jones formula was widely studied because of its simplicity. On the other hand, it is incapable of accurately describing specific material's properties for instance, metals, which would be overcome by many body potentials such as embedded atom method potential (EAM). However, regardless of how well it is able to model actual materials, Lennard-Jones potential is the standard potential to use for all investigations where the focus is fundamental issues, rather than studying the specific properties of one kind of material. The simulation work done using Lennard-Jones potential helped us to

understand basics in many areas of condensed matter physics, and for that, the importance of it cannot be underestimated.

Some two-body potential such as Morse potential[103], revised Morse-John potential were also employed to study metals.

2.2.2 Many body potential – Embedded Atom Method Potential

As the name suggested, many body potentials take additional atoms interaction into consideration while describing interatomic relationships. EAM [104] is one of the important types of many body potentials that was used in the current thesis study. EAM is constructed by a pairwise term and a local electron density term describing the N-body interaction that is widely employed in the computational studies of metals. Generally speaking, many-body potential is more accurate in describing interatomic interactions and demanding more computational sources.

EAM was first developed by Daw and Baskes [104]. In EAM potential, each atom in a solid is considered an impurity and all other atoms are viewed as the host in which the atom is embedded. The energy of the impurity, embedded energy, is a function of the background electron density. The energy of the host is a function of the impurity type and position. The sum of above two parts is the total potential energy expressed as follows:

$$E_{tot} = \sum_i F_i(\rho, i) + \frac{1}{2}\sum_i \sum_{j \neq i} \phi_{ij}(R_{ij}) \qquad [2.2.1]$$

And

$$\rho, i = \sum_{i \neq j} \rho_j^a(r_{ij}) \qquad [2.2.2]$$

where ρ,i is the host electron density at atom i, $F_i(\rho,i)$ refers to the energy required for embedding an atom i into uniform electron density ρ,i , while ρ,i is the spherically averaged atomic electron density at atom site i created by all of the rest atoms in the system. $\phi_{ij}(R_{ij})$ is pair wise potential between atom i and j with a separation distance r_{ij}.

With the consideration of electron density, EAM potential has been proved to be effective in simulating metals. The exact form of EAM used in this thesis study is Carter [105] form of EAM [106] potential for Fe-H. This potential is based on the EAM potentials of α iron Mendelev et al. [107] and Ackland et al. [108] and an extensive database of energies and atomic configurations from density functional theory (DFT) calculations have been fit the cross interaction of H and Fe.

2.3 Integration Algorithm

The potential energy is a function of the atomic positions (3N) of all the atoms in the system. In light of the complicated nature of this function, they must be solved numerically.

The time integration algorithms are based on finite difference methods, whereby time is discretized on a finite grid, the time step Δt being the distance between consecutive points on the grid. Knowing the positions and some of their time derivatives at time *t*, the integration gives the same quantities at a later time step $t + \Delta t$. By iterating the process, the time evolution (trajectory) can be obtained for a long time. The intrinsic error that comes from finite difference methods is truncation errors as only limited terms of Taylor expansion were used.

To integrate the equation of motion, several numerical algorithms have been developed. They are listed here.

- Verlet algorithm
- Velocity Verlet algorithm
- Leap-frog algorithm
- Predictor – corrector algorithm

As Velocity Verlet algorithm is used in this thesis study, Verlet and Velocity Verlet algorithms are the only ones to be introduced here.

2.3.1 Verlet Algorithm

One of the most commonly used integration algorithms in molecular dynamics is the Verlet algorithm[109]. The basic idea is to use two third-order Taylor expansions for the positions $r(t)$, one forward and one backward in time.

$$r(t+\Delta t) = r(t) + v(t)\Delta t + (1/2)a(t)\Delta t^2 + (1/6)b(t)\Delta t^3 + O(\Delta t^4) \qquad [2.3.1]$$

$$r(t-\Delta t) = r(t) - v(t)\Delta t + (1/2)a(t)\Delta t^2 - (1/6)b(t)\Delta t^3 + O(\Delta t^4) \qquad [2.3.2]$$

where v is the velocity, a is the acceleration, b represents the third derivative of r with respect to t. Adding the above two expressions gives

$$r(t+\Delta t) = 2r(t) - r(t-\Delta t) + a(t)\Delta t^2 + O(\Delta t^4) \qquad [2.3.3]$$

This is the basic form of the Verlet algorithm. The acceleration $a(t)$ is just the force divided by the mass, and the force is a function of potential with respect to the position $r(t)$.

$$a(t) = -(1/m)\nabla V(r(t)) \qquad [2.3.4]$$

The truncation error of this algorithm when evolving the system by Δt is of the order of Δt^4. This algorithm is simple to implement, accurate and stable. However the equation only has positions, therefore, was refereed as position Verlet algorithm. In practice, we need velocities to calculate quantities such as the kinetic energy, temperature, and correlation functions involving velocities. Therefore, in position Verlet algorithm, velocity is obtained from the positions as the following equation:

$$v(t) = \frac{r(t+\Delta t) - r(t-\Delta t)}{2\Delta t} + O(\Delta t^2) \qquad [2.3.5]$$

The accuracy of obtained velocity is on the order of $O(\Delta t^2)$. To overcome this difficulty, modifications of the basic Verlet scheme

have been proposed such as Beeman algorithm, velocity-corrected Verlet algorithm which are not introduced here. However, due to its simplicity and acceptable level of accuracy, Verlet algorithm is most widely used in MD simulations.

2.3.2 Velocity Verlet Algorithm

Velocity- Verlet algorithm[110] is a better scheme where positions, velocities and accelerations at $t+\Delta t$ are obtained from the same variables at time *t*. Equations are as follows.

$$r(t+\Delta t) = r(t) + v(t)\Delta t + (1/2)a(t)\Delta t^2 \qquad [2.3.6]$$

$$v(t+\Delta t/2) = v(t) + (1/2)a(t)\Delta t \qquad [2.3.7]$$

$$a(t+\Delta t) = -(1/m)\nabla V(r(t+\Delta t)) \qquad [2.3.8]$$

$$v(t+\Delta t) = v(t+\Delta t/2) + (1/2)a(t+\Delta t)\Delta t \qquad [2.3.9]$$

Combining eq.[2.3.7]and eq.[2.3.9] yields

$$v(t+\Delta t) = v(t) + (1/2)(a(t+\Delta t) + a(t))\Delta t \qquad [2.3.10]$$

The basic forms of Velocity Verlet are eq. [2.3.6] and [2.3.10]. The deduction process above has shown that the accuracy of velocity is on the order of $O(\Delta t^4)$ which is superior to Verlet algorithm. Manipulations of equations would yield the same trajectory equation as position Verlet. Therefore, the accuracy Velocity Verlet integrator is the same as position Verlet algorithm. In addition, Velocity Verlet algorithm allows the position and velocity to be automatically

synchronized comparing to position Verlet algorithm. Velocity Verlet is used in this thesis study. Other algorithms were discussed in details in reference[97].

Attention should be given to the choice of the time step Δt. In this study, the time step is chosen in the way that it's smaller than the fastest vibration frequency in this system, which is the vibration frequency of atoms, so the motion of atoms can be captured. The typical order of the atomic vibration frequencies is 10^{14} Hz. Thus, the time step is chosen as 10^{-15} s.

2.4 Temperature control

Temperature control in classical MD simulation is based on statistical mechanics. MD simulation performs with microcanonical ensemble (or NVE ensemble) which has the number of atoms, the volume of the system and total energy conserved. In this thesis, NVT ensemble (canonical ensemble) was also used as a way of relaxing simulation system while keeping the number of atoms in the system, the volume, and the temperature constant. The method employed to maintain a constant temperature is illustrated below.

There are mainly several methods controlling temperature in MD simulations and introduced as follows.

2.4.1 Stochastic methods

This method corresponds to coupling the simulation system to an imaginary heat bath to achieve desired constant temperature. The coupling is done through stochastic impulsive forces or called collisions. At intervals, the velocity of a randomly selected molecule is changed to a random pick from Maxwell-Boltzmann distribution at the desired temperature. This corresponds to a collision. One of the most famous this kind methods is called Anderson thermostat[111]. The times between collisions with the bath are random.

Alternative to Anderson thermostat is to resample the velocities of all particles in the system from Maxwell-Boltzmann distribution at regular points in time such as every *n* steps[112].

2.4.2 Extended system method

Another way of treating the simulation system coupling to a thermal bath is to introduce an extra degree of freedom that represents the heat bath and carry out with a simulation of this "extended system".

One of such methods is known as Nose thermostat[113] where additional fictitious coordinate is added to Lagrangian and the equation of motion is solved. This method is more "gentle" comparing to other collision methods where random changes in velocities occurred. Here we provide a brief introduction of the Nose formulism.

The extra degree of freedom is denoted as s which is dimensionless, and it has a conjugate momentum p_s.the real velocities are related to the time derivatives of position by

$$v = s\dot{r}_i = p / m_i s \qquad [2.4.1]$$

Potential energy associated with s is

$$V_s = (f+1)k_B T \ln s \qquad [2.4.2]$$

Where f is the number of degrees of freedom i.e. 3N in a 3D system and T is the specified temperature.

The kinetic energy term is

$$K_s = \frac{1}{2}Q\dot{s}^2 = \dot{p}_s^2 / 2Q \qquad [2.4.3]$$

Where Q is the thermal inertia that controls the rate of temperature fluctuation.

The Lagrangian of the system is

$$\begin{aligned} L_{Nose} &= K - V + K_s - V_s \\ &= \sum_{i=1}^{n} \frac{m_i}{2} s^2 \dot{r}_i^{\,2} - V(r) + \frac{Q}{2}s^2 - (f+1)k_B T \ln s \end{aligned} \qquad [2.4.4]$$

Taking time derivatives with respect to $\frac{\partial L_{Nose}}{\partial \dot{r}}$ and $\frac{\partial L_{Nose}}{\partial \dot{s}}$ yields the following equations

$$\ddot{r} = f / m_i s^2 - 2\dot{s}\dot{r}_i / s \qquad [2.4.5]$$

$$Q\ddot{s} = \sum_{i}^{n} m\ \dot{r}_i^{\,2} s - (f+1)\mathrm{k}_B T / s \qquad [2.4.6]$$

The extended system Hamiltonian $H_s = K + K_s + V + V_s$ is conserved. The density function of the extended system is microcanonical which means the energy of extended system is conserved while the system follows canonical distribution maintaining a constant temperature.

$$\rho_{NVE_s}(r, p, s, p_s) = \frac{\delta(H_s - E_s)}{\int drdpdsdp_s \delta(H_s - E_s)} \qquad [2.4.7]$$

Nose –Hoover method is a method Hoover developed by extending Nose's method in 1985[114]. Then it became very widely employed. In this study, Nose – Hoover method is used.

2.4.3 Constraint methods

Velocity rescaling is a method based on velocity – temperature relationship from statistical mechanics as shown below:

$$< \sum_{i=1}^{N} \frac{1}{2} m v_i^{\,2} >= \frac{3}{2} N k_B T \qquad [2.4.8]$$

where m is the mass, v_i is the velocity of atoms i, N is the number of atoms in system; k_B is the Boltzman constant and T is the system temperature. As the system evolves with time, the instantaneous temperature at each time step T_i could be obtained through equation above by calculating velocities of all atoms. Thus, rescaling the

velocities at each time step by a factor of $\sqrt{\frac{T}{T_i}}$ would achieve the desired temperature for the system. Velocity rescaling is a crude method of solving a set of equations of motions that disturbs the dynamics of the system, thus, it is normally used to equilibrate a system before starting a simulation.

2.5 Pressure control

In this thesis study, uniaxial tensile test were performed. Strains were applied along tensile direction on the surface of the simulation box where a few layers of atoms were kept fixed as a gripping part. The other two dimensions were controlled to be stress-free to mimic uniaxial loading condition of a real tensile test. Therefore, the isothermal-isobaric ensemble (NPT) was employed.

Various schemes for prescribing the pressure of a MD simulation have also been developed. In all of these methods it is inevitable that the simulation box must change its volume to maintain a constant pressure. A brief introduction is provided.

2.5.1 Extended system methods

Like the method used in temperature control scheme, an extra degree of freedom is introduced to mimic a piston on a real system. Thus, this method involves coupling the simulation system to an external variable, the volume of the simulation box. Through

adjusting the "piston", the volume of the system is changed to maintain constant pressure.

2.5.2 Changing box-shape

Anderson developed a constant-pressure method in 1980 which allows for isotropic changes in the volume of the simulation box[111]. Parrinello and Rahman [115,116] extended this method to allow the simulation box to change size as well as shape. This technique is particularly useful in the study of solids as it allows for phase changes in the simulation which may involve the changes in unit cell dimensions and angles[97].

A time dependent metric tensor that allows the volume and shape of the MD simulation box to vary with time was introduced. The edges of the simulation box are denoted as three vectors, a, b and c. h is defined as the matrix formed by $\{a,b,c\}$; $\Omega = a \bullet b \times c$ is the volume of the simulation box with N particles. The position of particle I is $r_i = hs_i = l_i a + m_i b + n_i c$ where s_i has components (l,m,n) each going from 0 to 1. Then $r_i^2 = s_i^T G s_i$ where superscript T denote transpose and $G = h^T h$. The Lagrangian is

$$L = \frac{1}{2}\sum_{i=1}^{N} m_i s_i^T G s_i - \sum_{i=1}^{N}\sum_{j>i}^{N-1} \phi\,(r_{ij}) + \frac{1}{2} W Tr(h^T h) - p\Omega \qquad [2.4.9]$$

p denotes the pressure, W has the dimension of mass. This Lagrangian generates a NPH ensemble where H refers to enthalpy.

Simulations in this thesis study use the Gibbs ensemble (NPT) which combined the Parrinello-Rahman method [115] for controlling the zero pressure along non- tensile directions, and the Nose-Hoover method [113] for maintaining constant temperature.

2.6 Periodic boundary condition

Computer simulation is normally performed on a small number of atoms or molecules, i.e., 10 to 10000. The size of the system is limited by the storage capacity and, more crucially by the speed of execution of the program. If we are only interested in the properties of a very small cluster of atoms or molecules, or a microcrystal, simulation would be very straightforward. However, if our interest lies in bulk of materials, the limitation of size of simulation box would cause a problem[97]. In addition, the ratio between the number of surface (where the simulation system terminates) atoms and the total number of atoms would be much greater than in reality, resulting surface effects to be much more influential than what they should.

To match the practical scale in reality, a very large system of atoms needs to be modeled to study macroscopic phenomena such as hydrogen embrittlement. However, even with the super computation power, only a very small system with limited number of atoms (less than 10^9 atoms) can be simulated with a significant cost. This is still negligible comparing with the number of atoms contained in a macroscopic piece of matter (of the order of 10^{23}). A solution to solve the size limitation and surface impact is to use periodical boundary

condition (PBC) [117]. When using PBC, particles are enclosed in a simulation box and we imagine that this box is replicated to infinity by rigid translation in all the three Cartesian direction, completely filling the 3 dimension space. For instance, if one particle is located at position r in the simulation box, this particle actually refers to all particles located at

$$r + l \cdot a + m \cdot b + n \cdot c$$

where l, m, n are integer numbers and a, b, c are the box length along three edges of the simulation box. All of them move simultaneously and only one of them is represented in the program.

PBC introduces an infinite space-filling array of identical copies of the simulation region. By using PBC, each particle i in the box interacts not only with other particles j but also interacts with their images in nearby box. The interactions "go through" box boundaries. Apparently the number of interacting pairs increases enormously as a result of the effect of PBC. In practice, potentials usually have a cutoff distance where short interaction range is defined. It is called minimum image criterion which reduced additional complexity introduced by employing PBC. More details of PBC and minimum image criterion should be sought in reference[97].

2.7 Pressure calculation

Each atom has 6 components of its stress tensor calculated and stored in files. The cube in Fig.2.2 is an imaginary element of a

material in three dimensions. There is one normal stress perpendicular to the plane and two shear stresses on the plane as shown. For example, the surface with normal vector in the direction of y-axis, the normal stress is denoted as σ_{yy}, the first letter refers to the plane and the second letter refers to the direction of the vector. The other two shear stress components are τ_{yx} and τ_{yz}. Thus, there are totally six stress components. They are calculated using the following equation in LAMMPS code[118].

$$S_{ab} = \frac{-[mv_a v_b + \frac{1}{2}\sum_{i=1}^{N_p}(r_{1a}F_{1b} + r_{2a}F_{2b})]}{V_{atom}} \qquad [2.4.10]$$

where subscripts a and b could be replaced by x , y and z to get the total six stress tensors. In the equation, the first term is a kinetic energy contribution for atom I. The second term is a pairwise contribution where i loops over N_p neighbors of the atom. r_1 and r_2 are the positions of two atoms in the pairwise interaction. F_1 and F_2 are the forces on the two atoms resulting from the pairwise interaction. V_{atom} refers to the volume of a specific atom being calculated.

In this thesis study, pressure is calculated to characterize the location of initially created dislocations and facilitate the analysis of final results to have a better understanding on stress state of the system. The pressure is calculated by

$$P = -(\sigma_{xx} + \sigma_{yy} + \sigma_{zz})/3 \qquad [2.4.11]$$

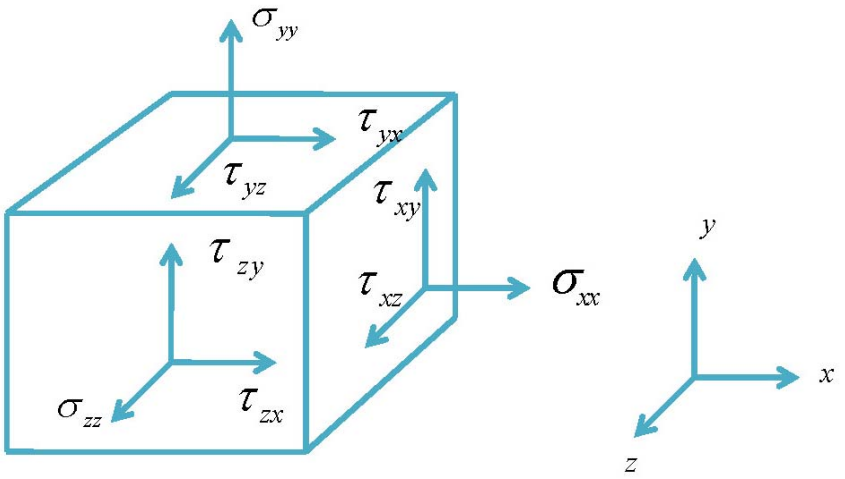

Fig. 2.2 Stress tensors in three dimentions.

2.8 Simulation model set up

In order to investigate the interaction between hydrogen and edge dislocations, the first step is to create a model filled with edge dislocations. It is a three-step process. First of all, we created a three-dimensional body-centered cubic α-Fe single crystal with a dimension of about 5 x 20 x 26 nm oriented with crystallographic directions [100], [010] and [001] in the X-, Y- and Z-directions, respectively as shown in Fig. 2.3.

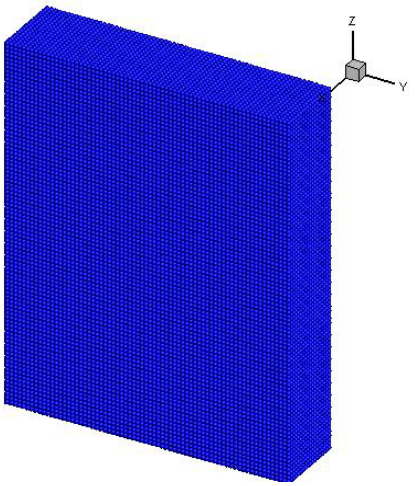

Fig. 2.3 Perfect 3D body-centered-cubic model composed by iron atoms colored in blue

The single crystal consists of approximately 220000 atoms. We apply periodic boundary conditions along X- and Y- directions and free boundary condition along Z-direction which is chosen as the uniaxial tensile loading direction. The second step is to perform a thermal relaxation of this newly created model at T = 300K for 2 nano-seconds (ns). The third step is to apply a uniaxial tensile loading to the model to deform the single crystal into plastic region (up to > 8%) in order to create dislocations as shown in Fig. 2.4.

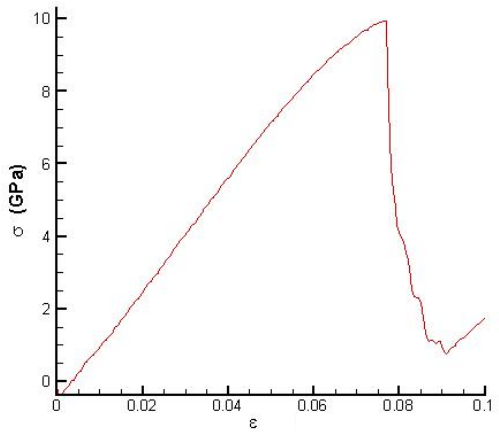

Fig. 2.4 Stress strain curve from initial tensile simulation

During deformation, zero pressure conditions were applied in the X- and Y-directions and continuous displacement was applied in the Z-direction by fixing a few layers of atoms at one end and extending a fixed grip of atoms at the other end at a constant velocity of 1m/s. The time step in MD simulation of this study is 10^{-15} s. Right after the plastic deformation, we released the loading and repeated the thermal relaxation at T = 300K for 4 ns to obtain equilibrium defects structure. Figure 2.5 shows the three dimensional atomic configuration of the system after relaxation where the atoms are colored by pressure followed by a two-dimensional configuration in Figure 2.6. Red is compressive pressure, blue is tensile pressure.

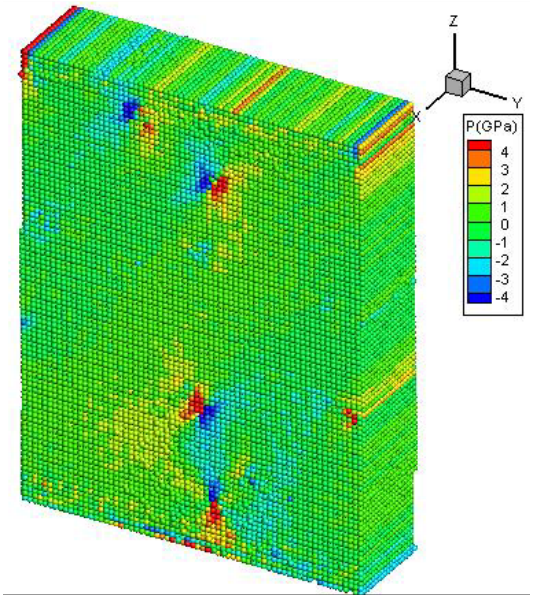

Fig. 2.5 Three dimension hydrogen free model filled with edge dislocations colored by pressure.

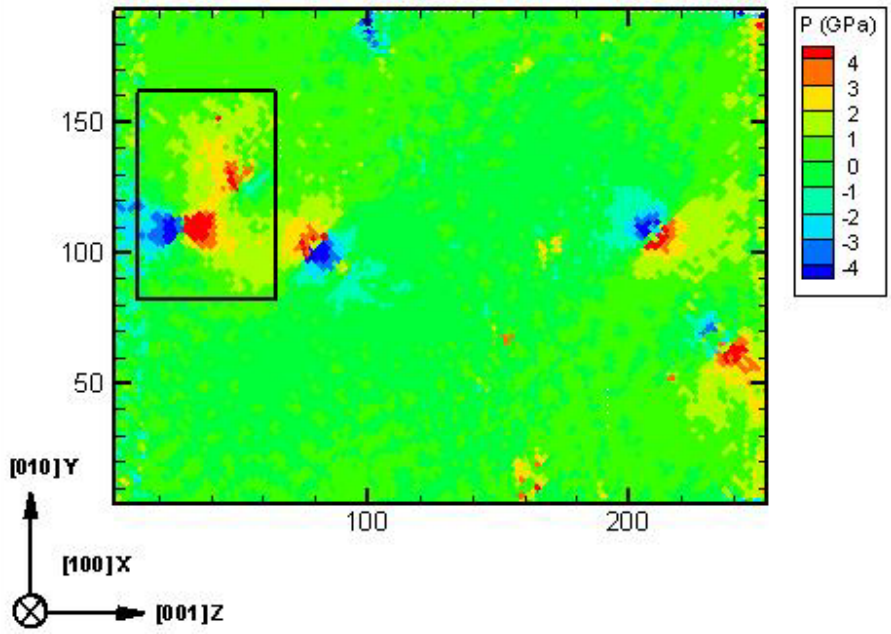

Fig. 2.6 2D Atomic stress (pressure) distribution of simulation cell without Hydrogen. Red is compressive pressure, blue is tensile pressure.

Evidently, a total of five edge dislocations were generated after this procedure. Four of them are clearly visible in Fig. 2.5 while another one is more visible in Figure 2.6 within the black rectangular. Two types of edge dislocations were found with Burger's vectors of $a[010]$ (introduced during the procedures of relaxation and rigid layers treatment) and $a/2[0\bar{1}\bar{1}]$, where a = 2.8607 Å is the equilibrium lattice parameter at T = 300K. Because of the constraint of the periodic boundary conditions, the dislocations generated from plastic deformation are all having the dislocation lines along X-direction (or [100] crystallographic direction), which is perpendicular to the Y-Z plane, and consequently, it prevents the formation of the <111> type

of dislocations that are commonly observed in α iron in experiments. It is also worth noting the total Burgers vector is not conserved in current simulation cell, suggesting the existence of step along Y-direction. The dislocation density is estimated to be 10^{16} m^{-2}, which is the upper limit of dislocation density of highly deformed metals such as cold-rolled or fatigued bcc Fe and its alloys [119,120].

At this stage, a hydrogen free model with edge dislocations has been created. In order to test the effect of varying hydrogen concentration, different level of hydrogen content was deposited in the hydrogen free model to form new models. Based on the fact that hydrogen thermodynamically prefers to stay at the tetrahedral interstitial sites rather than the octahedral interstitial sites [51,54,121-126] concluded from the majority of studies so far, hydrogen atoms were randomly deposited into bcc tetrahedral interstitial sites in the simulation cell, followed by a thermal relaxation (NVE ensemble) at T = 300K for 2 ns. Thus, 13 models with different hydrogen concentration levels from 0 % to 6.2 % (atomic percentage) were then created.

MD simulations of uniaxial loading tests were then performed using the Gibbs ensemble on all 13 models. This method combined the Parrinello-Rahman method [115] for controlling the zero pressure along X- and Y- directions, and the Nose-Hoover method [113] for maintaining constant temperature. The uniaxial tensile loading is applied by fixing a few layers of iron atoms in one end of the simulation box along Z direction and displacing the similar

counterpart in the other end of the simulation box at a constant velocity of 1 m/s. It is worth noting that no hydrogen atoms have been placed in these two fixed gripping regions. The interatomic interaction was described using Carter [105] form of the Embedded Atom Method (EAM) [106] potential for Fe-H. All simulations were carried out using LAMMPS code [118].

To make simulation process of this study more illustrative, the following schematic is shown below.

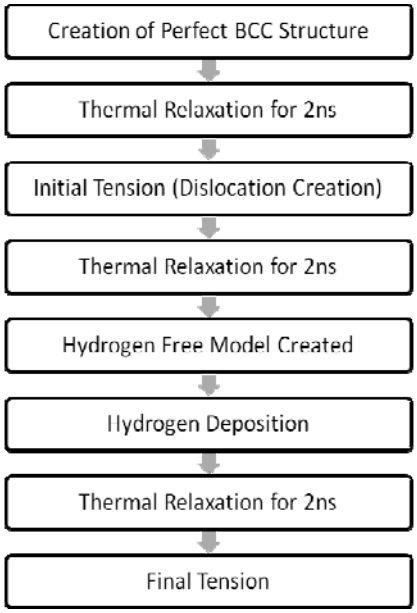

Fig. 2.7 Simulation process schematic

3 Hydrogen hardening mechanism

Based on the comparisons of 13 cases simulations which employed different level of hydrogen concentrations, we concluded that hydrogen induced hardening which was demonstrated by the

rising yield stress as the effective hydrogen concentration increases. The following chapter would explain the intrinsic mechanism of this phenomenon.

3.1 Hydrogen diffusion in heavily deformed iron crystal

Hydrogen atom has a tendency to bind with materials defects to lower the total energy. The calculation of trapping energy of hydrogen to dislocations or segregation energy of hydrogen to other crystal defects [58,66,105,127] suggest that in the heavily deformed iron crystal hydrogen will diffuse toward edge dislocations and other crystal defects at room temperature. Figure 3.1 shows hydrogen concentration profile along Z direction at three different levels of time. For the sake of clarity, a simulation case with higher hydrogen concentration was chosen. The horizontal straight line at 2% represents the average hydrogen atomic percentage. At early time (t = 0 picoseconds) in Fig.3.2, the hydrogen atoms are evenly distributed along Z-direction in the system. However, multiple peaks develop at later time, where the peak positions correspond to the locations of edge dislocations in Z-directions. Meanwhile the region surrounding each peak shows depleted hydrogen concentration as shown in Fig. 3.3 (t = 500 picoseconds) and Fig. 3.4(t = 3000 picoseconds).

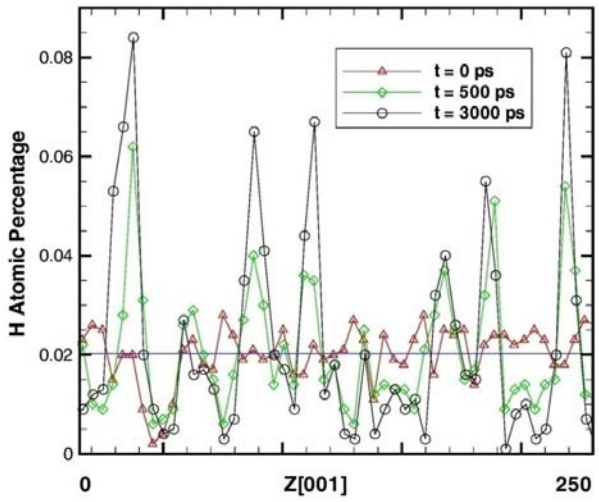

Fig. 3.1 Hydrogen concentration profile along Z-direction at three different times

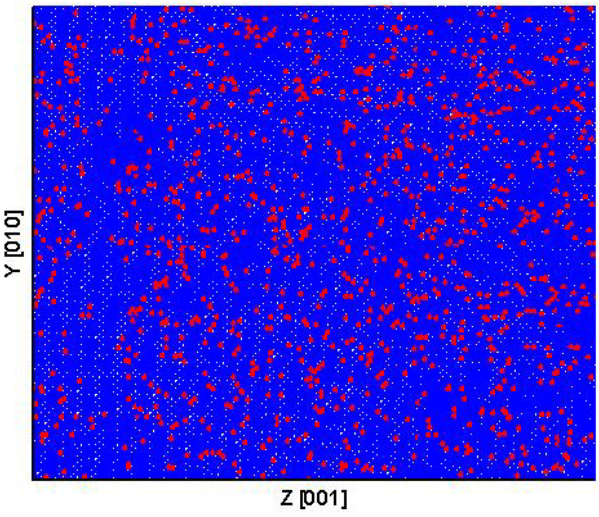

Fig. 3.2 2D hydrogen distribution diagram at the begin of the simulation corresponding to t = 0 ps in Fig. 3.1. Red refers to hydrogen atoms, blue refers to iron atoms.

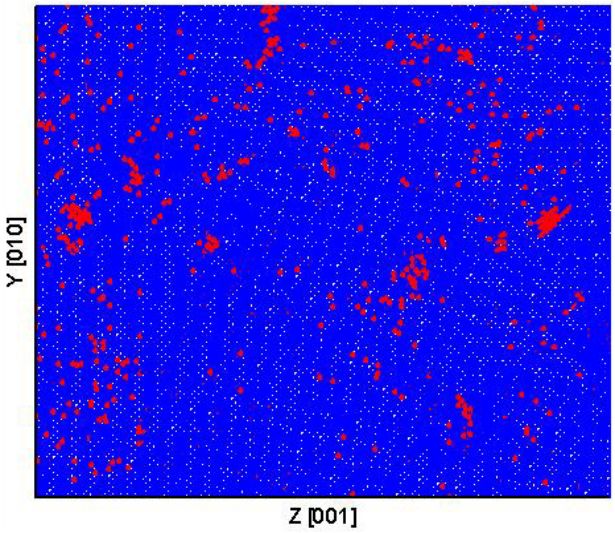

Fig. 3.3 2D hydrogen distribution diagram corresponding to t = 500 ps in Fig. 3.1

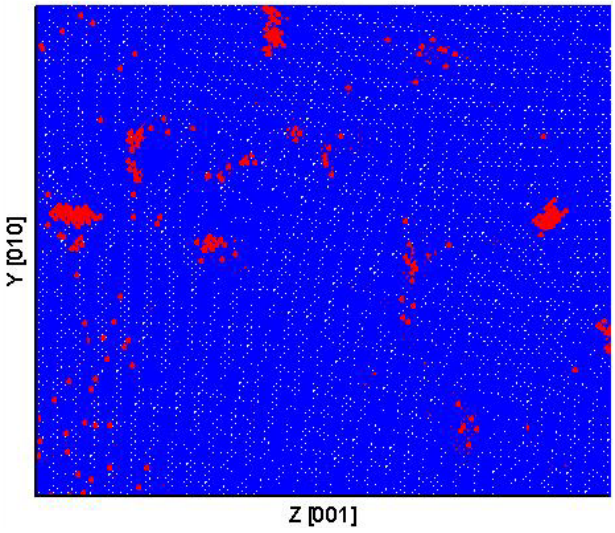

Fig. 3.4 2D hydrogen distribution diagram corresponding to *t* = 3000 ps in Fig. 3.1

Through comparisons of figures above, it confirms that hydrogen atoms have tendency to diffuse into crystal defects and are trapped within these defects. This is also consistent with our previous MD simulations of hydrogen diffusion in the bulk, vacancies and grain boundaries in α-iron[58]. Note there are more than five peaks displaying along Z-direction, which suggests that some of the peaks do not correspond to the location of dislocations. The origin of these corresponds to the existence of other crystal defects such as vacancies or local structure disorder in the iron crystal. The magnitude of peaks in the figure qualitatively described the trapping ability among dislocations, vacancies and other disordered local structures.

3.2 Dislocation motion and hydrogen pinning during deformation

Figure 2.6 shows the atomic configuration of the simulation cell after relaxation, where the atoms are colored by pressure in GPa. The red indicates the compressive while the blue refers to the tensile pressure. As shown in Fig. 2.6, each dislocation is associated with one tensile stress and one compressive stress field separated by a slip plane. Figure 3.5 shows an enlargement of a small part in the black rectangular in Figure 2.6, where two dislocations are shown. The Burgers vectors of these two edge dislocations are determined using Burgers circuit, as shown in Fig. 3.5. We found the Burger's vectors of these two dislocations are $a[010]$ and $a/2[0\bar{1}\bar{1}]$, respectively. Similarly, we determine that the rest three dislocations are with

Burgers vectors of $a/2[0\bar{1}\bar{1}]$, $a/2[011]$ and $a/2[011]$. Hence two types of edge dislocations have been generated after the initial deformation. Since the uniaxial loading is along [001] crystallographic direction and no resolved shear stress will be applied to the dislocation with Burgers vector of $a[010]$, the dislocation will not move during deformation. However, the other four dislocations with $a/2[011]$ type of Burgers vector will have the potential to glide due to the resolved shear stresses.

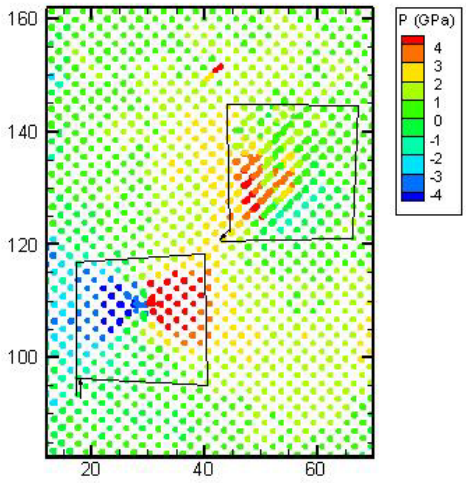

Fig. 3.5 Atomic configuration of the enlarged area in Fig.2.6. Atoms are colored by pressure. Red is compressive pressure, blue is tensile pressure.

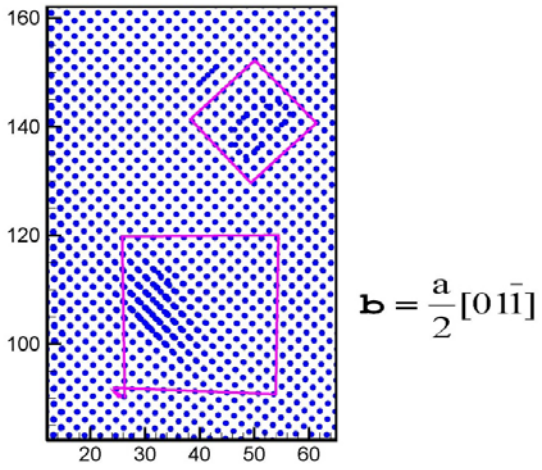

Fig. 3.6(a) Atomic configuration of the same enlarged area in Fig.2.6 (a) in the case of hydrogen free at ε= 0.2% (after yielding).

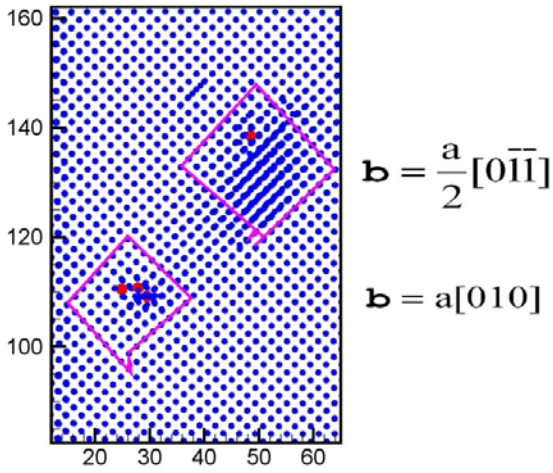

Fig. 3.6(b) Atomic configuration of the partial simulation cell. (the same enlarged area in Fig.2.6 (a)) in the case of 10 hydrogen at ε = 0.2% (before yielding)

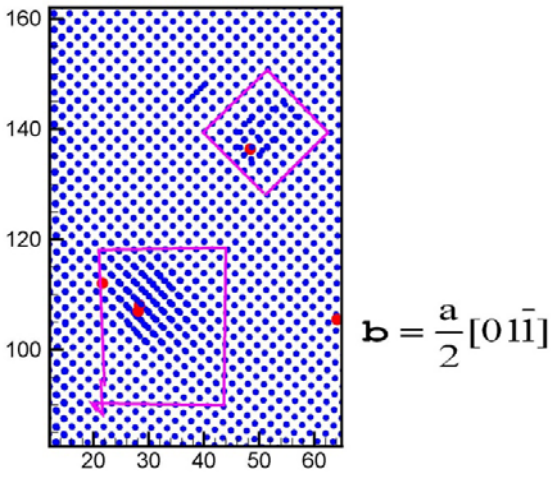

Fig. 3.6(c) Atomic configuration of partial simulation cell (the same enlarged area in Fig.2.6 (a))in the case of 10 hydrogen at ε=0.3% (after yielding). The red circles indicate hydrogen and blue circles denote iron atoms. Burgers' circuit has been highlighted in pink.

To better understand how hydrogen interacts with dislocations during deformation, we performed MD simulation of uniaxial tensile tests with and without hydrogen. As expected, in both cases after yielding the dislocations with ***b***= $a/2[0\bar{1}\,\bar{1}]$ glide along slip plane for some extent, while the dislocation with ***b***= $a[010]$ keeps immobile. More specifically, the dislocation ***b***= $a/2[0\bar{1}\,\bar{1}]$ will glide toward the dislocation ***b***= $a[010]$ and combine according to the reaction $a[010]+a/2[0\bar{1}\,\bar{1}]\rightarrow a/2[01\bar{1}]$ to form a new dislocation with ***b***= $a/2[01\bar{1}]$. The occurrence of this dislocation reaction is independent of the existence of hydrogen in α iron crystal. This reaction has been observed for all cases with different level of hydrogen concentration.

Figure 3.5 has shown the same enlarged area in Fig. 2.6 while using different color to illustrate the relative location of Fe atoms (blue) and hydrogen atoms (red). Figure 3.6 (a) shows the atomic configuration of the same enlarged area in Fig. 2.6 in the hydrogen free case after yielding with a strain of approximately 0.2%. The yield strength for the single crystal iron without charged hydrogen is estimated to be 0.32 GPa. It is clear that after yielding two dislocations have been recombined to form a new dislocation with $\boldsymbol{b}=a/2[01\bar{1}]$.

Figure 3.6 (b) shows the atomic configuration of the same enlarged area in Fig.3.5 In the case of 10 hydrogen atoms at the strain of approximately 0.2%, where the red circles indicate hydrogen and blue circles denote iron atoms. Note that the same stress level, which can cause yielding for the model without hydrogen, could not initiate dislocation gliding when hydrogen is present. Indeed, the yield strength for the single crystal iron with 10 charged hydrogen atoms is estimated to be 0.5 GPa. This implies that higher resolved shear stress is required to move dislocations when hydrogen is present. Figure 3.6 (c) shows the atomic configuration of the model with 10 hydrogen atoms at the strain of approximately 0.3%. Apparently, yielding has occurred by the reaction of the two edge dislocations and the formation of the new dislocation. Since the dislocation $\boldsymbol{b}=a[010]$ is immobile, the only reason that the yield strength is different between these two cases is the presence of one hydrogen atom within $\boldsymbol{b}=a/2[01\bar{1}]$ dislocation core. We believe that hydrogen atom acted as a

pinning point when it was trapped within a dislocation core. The pinning hindered the motion of the dislocation, thus, a higher resolved shear stress is required to overcome hydrogen-induced pinning, leading to an observation of macroscopic hardening. This pinning effect can be understood in the general framework of solid solution dragging of dislocations, where the existence of solid solution can energetically lower the dislocation energy, in turn, increase the Periels stress that requires to initiate the motion of dislocations[128,129]. Our finding of hydrogen pinning effect supports the previous hypothesis that hydrogen trapped in dislocations could increase critical shear stress of gliding and pin edge dislocations [33].

It is also interesting to observe how hydrogen interacts with dislocation during the yielding. As shown in Fig. 3.6 (b), before yielding the hydrogen atom was trapped in the dislocation core. However, as seen in Fig. 3.6 (c), after yielding, instead of gliding with the dislocation, the hydrogen atom has been de-associated from the dislocation. The dislocation velocity can be estimated simply by taking the dislocation core displacement within a time interval *t* after yielding. This value is approximately 1200 m/s, which is close to the value in literature where the velocity of $1/2[111](1\bar{1}0)$ edge dislocation under stress ranging from 30MPa to 1000MPa at 300K were studied [130]. However, based on the hydrogen diffusion in alpha iron [58], the movement of hydrogen is much lower than the movement of dislocations. This movement difference is a reflection of hydrogen – dislocation de-association process. It is also worth noting that the movement difference between hydrogen diffusion and dislocation

motion could be attributed to the extremely high strain rate (~10^7 s^{-1}) in typical molecular dynamics simulation. This also suggests that the increase in yield strength might be related to the additional force required breaking the binding between dislocation and hydrogen. In summary, direct observations of hydrogen-induced pinning effect strongly support the previous findings[15,85]. Hydrogen pinning dislocation model was observed which was concluded by Murakami et al [15] based on studies of Moriya et al. [32]. Additionally, the simulation work by Nedelcu et al. also concluded hydrogen pinning effect on edge dislocations [85].

The obstacles created by hydrogen trapped in dislocation core contribute to higher yield strength, and consequently, the occurrence of hardening effect.

3.3 Effect of hydrogen concentration on yield strength

It is found that yield stress of all 13 cases did not follow common postulate that the higher hydrogen concentration leads to higher pinning effect which induced higher yield stress. However, closer examination yields the notion of effective hydrogen concentration. Figure 3.7 shows yield strength of the single crystal iron as a function of effective hydrogen concentration. Each data point is averaged over three independent simulations and the uncertainties are based upon a 95 % confidence interval. Here, we define the effective hydrogen concentration C_{EH} as the number of hydrogen atoms per unit length along a dislocation core. Since only the

hydrogen atoms trapped in dislocations will have pinning effect, it is necessary to use the effective concentration rather than the nominal hydrogen concentration. For instance, in the case of 10 hydrogen atoms only 6 of them are trapped in 3 dislocations, resulting in a much lower effective hydrogen concentration than the nominal hydrogen atomic concentration.

While according to our observation the hydrogen atoms outside of dislocation cores do not contribute to the pinning effect; it is important to note that possible shielding effect of these hydrogen atoms to the nearby dislocation could ease the dislocation movement, thus leading to a local drop of yield strength. The inset of Fig. 3.7 shows a typical stress-strain curve and the yield strength of the single crystal is taken to be the stress at which the sudden drop of stress occurs. As shown in Fig. 3.7, the yield strength of the single crystal increases as the effective hydrogen concentration rises. In other words, the pinning or hardening becomes stronger as more hydrogen atoms are trapped in dislocation core.

This conclusion is explicitly expressed for the first time and directly observed in this study and is not inconsistent with previous findings[35,73,131] and has also confirmed the hydrogen pinning mechanism as suggested in references [15,32,132].

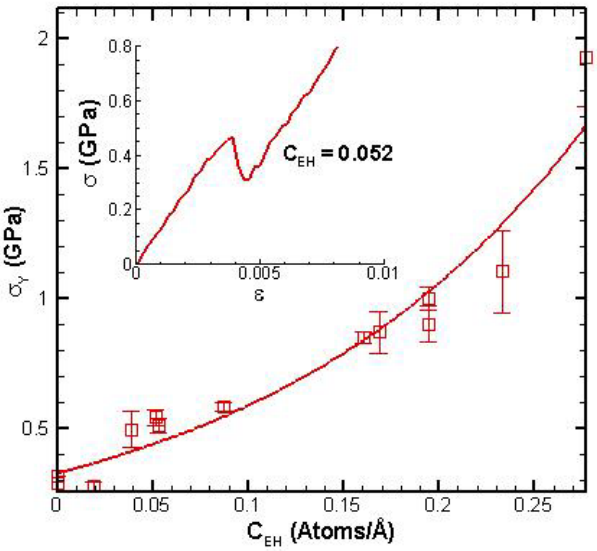

Fig. 3.7 Yield strength as function of effective hydrogen concentration in dislocation. A typical stress strain curve is shown in the inset.

3.4 Temperature dependence of pinning effect

To study how temperature affects the hydrogen – dislocation interaction process, simulations of hydrogen free and 10 hydrogen cases were performed at a temperature range of 250K to 350K.

Figure 3.8 shows the reciprocal of yield strength as a function of the reciprocal of temperature in a range of 250K to 350K for the case of hydrogen free and 10 hydrogen atoms. If the yielding is a thermally activated process, the inverse yield strength can be described as an Arrhenius function of temperature, as expressed by $\sigma_y = \sigma_y^0 \exp(Q/RT)$. Linear fitting of the data set to the equation allows us to extract the activation energy Q (from the slope) and the pre-

exponential factor σ_y^0 (from the intercept). Apparently, for hydrogen free case, the activation energy is negligible, which suggests that the initiation of edge dislocation is athermal. The rate of dislocation propagation is correlated to the stress applied, and the Peierls-Nabarro stress is reduced by a factor of [1-α (u^2/b^2)], where α is a numerical factor close to π, u is the mean atomic displacement and $\boldsymbol{b}$ is the Burgers vector [133]. In the temperature range we are interested, u is at most a few hundredths of $\boldsymbol{b}$ according to Lindemann's rule[134]. Consequently, the change in the Peierls-Nabarro stress with temperature will always be negligible, and so it is not surprising that the activation energy calculated for dislocation glide is close to zero. However, for the 10-hydrogen case, the activation energy is estimated to be 0.05 eV (4.82 KJ/mol) from the slope in Fig. 3.8, which suggests that the initiation of edge dislocation associated with de-pinning hydrogen is a thermally activated process. As indicated before, the increase in yield strength might be associated with breaking the binding between hydrogen and dislocation. Taketomi et al. [67] studied hydrogen-trap energy around {112}<111> edge dislocation using molecular static method and showed that the typical hydrogen-trap energy is on the order of 10^{-2} eV under zero shear strain condition, which is consistent with what we determined for the activation energy for dislocation glide. This implies that the de-association of hydrogen from dislocations is related to the breaking of the binding between hydrogen atoms and dislocation.

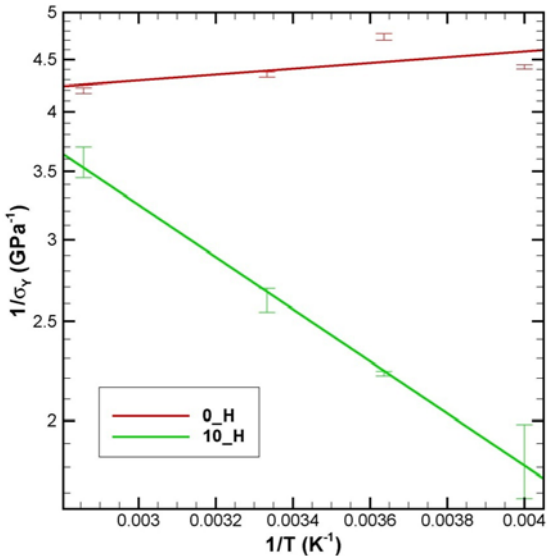

Fig. 3.8Yield strength as a function of temperature in the cases of hydrogen free and 10 hydrogen atoms.

3.5 Influence of vacancies around dislocation core on yielding

Since the yield strength is sensitive to the interaction between hydrogen and dislocations, it is reasonable to expect that any change around dislocation core will also lead to a change in yield strength. To confirm the speculation, we perform MD simulations of uniaxial tensile test under the condition where vacancies are introduced around one of the dislocation cores while the dislocation density and hydrogen concentration are kept constant. In particular, we take a simulation cell with four dislocations and 10 hydrogen atoms as a reference. Note that the four-dislocation model is a result of a plastic deformation in the original five-dislocation model where two of the dislocations combine to form a new dislocation. This reference model

is first relaxed at T = 300K for 1 ns and then subjected to a uniaxial tensile test. The yield strength measured in the reference model is 0.7 GPa. In order to introduce vacancies around dislocation core, we randomly remove 10% of Fe atoms in one of the mobile dislocations in the reference model, followed by a thermal relaxation at T = 300K for 1 ns. The yield strength is then determined to be 0.5 GPa. Since the only change between these two simulations is the vacancies density around one of the dislocations, the depression of yield strength could be attributed to the influence of interaction between vacancies and dislocations as well as interaction between vacancies and hydrogen. Previous studies have confirmed that the vacancies could enhance Fe – H bond at the expense of the exiting Fe –Fe bond, leading to decohesion [50,126,135]. Apparently, the weakened Fe-Fe bond is related to the lower yielding observed in this case.

4 Conclusion and future work

4.1 Conclusion

We have performed molecular dynamics simulations to investigate hydrogen-induced hardening/softening in a highly deformed alpha iron under uniaxial tensile loading. In particular, a network of edge dislocations was created as a result of plastic deformation of a perfect bcc iron single crystal. Possible factors that can influence the hydrogen-induced effect including effective

hydrogen concentration, temperature and vacancies around dislocation core were studied. The following results are obtained:

4.1.1 Hydrogen binding to crystal defects

During the process of depositing different level of hydrogen concentration into newly created deformed crystal structure that was filled with edge dislocations, hydrogen distribution was studied. Hydrogen binding to crystal defects was observed clearly. Hydrogen tends to bind with dislocations, vacancies and local disordered structure. The binding preference was qualitatively concluded as the sequence mentioned.

4.1.2 Hydrogen induced hardening effect on yield stress

Simulation results showed hydrogen-induced hardening as an evidence of increased yield strength is due to the dragging or pinning effect of hydrogen atoms in edge dislocations. Our studies have directly observed hydrogen pinning edge dislocations motion and are consistent with previous reported experimental observations [73,75,78,131,136,137] of hardening effect in terms of elevated yield stress or flow stress and reduced ductility.

4.1.3 Hydrogen pinning effect on edge dislocations

It is found that the yield strength of the single crystal iron monotonically increased with effective hydrogen concentration, which is defined as the number of hydrogen atoms per dislocation length.

This implied that the hardening was mainly caused by hydrogen dragging or pinning on the motion of dislocations.

4.1.4 Temperature effect on hydrogen pinning

The temperature dependence of yield strength in a hydrogen free system suggested that the initiation of dislocations is athermal. However, in the presence of hydrogen, the process is thermally activated and the activation energy was determined to be 0.05 eV, which is close to the hydrogen-trap energy, suggested by Taketomi [67] . Hence we believe that the increase in yield strength might be associated with the force required to break the binding between hydrogen and dislocation.

4.1.5 Effect of vacancies around dislocation core on yielding

In addition, the simulation of the effect of vacancies around dislocation core on hardening suggested that vacancies generated around dislocation weaken Fe-Fe bond in the presence of hydrogen, consequently, decreases the yield strength.

4.2 Limitation of current studies

Since the present simulations focused on a single crystal with particular crystallographic orientation described by an empirical

interatomic potential, embedded with very high density of edge dislocations and deformed with an extremely high strain rate, it is not yet possible to prove the generality of these observations. Nonetheless, the present results represent a direct observation of hydrogen pinning on edge dislocations that experiments are difficult to access at current stage.

4.3 Suggested the future work

Based on the limitations of this study, the following future work is suggested.

4.3.1 Crystallographic orientation & dislocation

Since the present simulations focused on a single crystal with particular crystallographic orientation X-[100],Y-[010] and Z-[001] with dislocations $a[010]$ and $a/2[0\bar{1}\bar{1}]$. To extend the generality of our conclusions, simulations of different types of edge dislocations should be performed.

4.3.2 Screw dislocation & temperature

Despite the fact that previous study has shown that at low temperature (lower than room temperature) hydrogen - screw dislocations interaction induce softening[32] , authors believe it is necessary to verify that results via simulation methodology and extend that conclusion to room temperature and high temperature domain.

4.3.3 Different microstructure

Simulations of ours were based on single crystal of α iron. Simulations of polycrystals should be conducted which includes grain boundaries and grains with different orientations. Other common impurities such as carbon in steels should be further considered in the future.

Reference:

1 Johnson, W. On some remarkable changes produced in iron and steel by the action of hydrogen and acids. *Proceedings of the Royal Society of London 1875, 23 ,(reproduced in "Hydrogen damage"). American Society for Metals, Ohio, 1977* (1875).

2 Vennett, R. M. & Ansell, G. S. Effect of High-Pressure Hydrogen Upon Tensile Properties and Fracture Behavior of 304l Stainless Steel. *Asm Trans Q* **60**, 242-& (1967).

3 Han, G., He, J., Fukuyama, S. & Yokogawa, K. Effect of strain-induced martensite on hydrogen environment embrittlement of sensitized austenitic stainless steels at low temperatures. *Acta Mater.* **46**, 4559-4570 (1998).

4 Toplosky, J. & Ritchie, R. O. On the Influence of Gaseous-Hydrogen in Decelerating Fatigue Crack Growth-Rates in Ultrahigh Strength Steels. *Scripta Metall Mater* **15**, 905-908 (1981).

5 Robinson, S. L. & Moody, N. R. The Effect of Hydrogen, Tritium and Decay Helium on the Fracture-Toughness of a Stainless-Steel Superalloy. *J Nucl Mater* **140**, 245-251 (1986).

6 Chen, W., Kania, R., Worthingham, R. & Van Boven, G. Transgranular crack growth in the pipeline steels exposed to near-neutral pH soil aqueous solutions: The role of hydrogen. *Acta Mater.* **57**, 6200-6214, doi:DOI 10.1016/j.actamat.2009.08.047 (2009).

7 Steigerwald, E. A., Schaller, F. W. & Troiano, A. R. The Role of Stress in Hydrogen Induced Delayed Failure. *Transactions of the American Institute of Mining and Metallurgical Engineers* **218**, 832-841 (1960).

8 Oriani, R. A. Hydrogen-Induced Crack-Propagation in Steels. *B Am Phys Soc* **19**, 219-219 (1974).

9 Oriani, R. A. & Josephic, P. H. Equilibrium Aspects of Hydrogen-Induced Cracking of Steels. *Acta Metall Mater* **22**, 1065-1074 (1974).

10 Lynch, S. P. Environmentally Assisted Cracking - Overview of Evidence for an Adsorption-Induced Localized-Slip Process. *Acta Metall.* **36**, 2639-2661 (1988).

11 Birnbaum, H. K. Hydrogen Effects on Deformation - Relation between Dislocation Behavior and the Macroscopic Stress-Strain Behavior. *Scripta Metallurgica Et Materialia* **31**, 149-153 (1994).

12 Birnbaum, H. K. & Sofronis, P. Hydrogen-Enhanced Localized Plasticity - a Mechanism for Hydrogen-Related Fracture. *Mat Sci Eng a-Struct* **176**, 191-202 (1994).

13 Board, N. E. Report of Public Inquiry Concerning Stress corrosion cracking on Canadian oil and gas pipelines. *MH-2-95, Calgary* (November 1996).

14 Song, J., Soare, M. & Curtin, W. A. Testing continuum concepts for hydrogen embrittlement in metals using atomistics. *Modell. Simul. Mater. Sci. Eng.* **18**, -, doi:Artn 045003

Doi 10.1088/0965-0393/18/4/045003 (2010).

15 Murakami, Y., Kanezaki, T. & Mine, Y. Hydrogen Effect against Hydrogen Embrittlement. *Metall Mater Trans A* **41A**, 2548-2562, doi:DOI 10.1007/s11661-010-0275-6 (2010).

16 Marchi, C. S., Somerday, B. P. & Robinson, S. L. Permeability, solubility and diffusivity of hydrogen isotopes in stainless steels at high gas pressures. *Int J Hydrogen Energ* **32**, 100-116, doi:DOI 10.1016/j.ijhydene.2006.05.008 (2007).

17 Beachem, C. D. New Model for Hydrogen-Assisted Cracking (Hydrogen Embrittlement). *Metallurgical Transactions* **3**, 437-& (1972).

18 Myers, S. M. *et al.* Hydrogen Interactions with Defects in Crystalline Solids. *Rev Mod Phys* **64**, 559-617 (1992).

19 Westlake, D. G. A Generalized Model for Hydrogen Embrittlement. *Asm Trans Q* **62**, 1000-& (1969).

20 Oriani, R. A. A Decohesion Theory for Hydrogen-Induced Crack Propagation *Stress Corrosion Cracking and Hydrogen Embrittlement of Iron Base Alloys, NACE-5* (1973).

21 Liu, H. W. Stress-Corrosion Cracking and Interaction between Crack-Tip Stress Field and Solute Atoms. *J Basic Eng-T Asme* **92**, 633-& (1970).

22 Vanleeuwen, H. P. Plateau Velocity of Scc in High-Strength Steel - Quantitative Treatment. *Corrosion* **31**, 42-50 (1975).

23 Owen, C. V. & Scott, T. E. Relation between Hydrogen Embrittlement and Formation of Hydride in Group V Transition-Metals. *Metall Trans* **3**, 1715-& (1972).

24 Westlake, D. G. Hydrogen Embrittlement - a Resistometric Study of Niobium(Columbium)-Hydrogen Alloys. *T Metall Soc Aime* **245**, 287-& (1969).

25 Simpson, C. J. & Ells, C. E. Delayed Hydrogen Embrittlement in Zr-2.5 Wt Percent Nb. *J Nucl Mater* **52**, 289-295 (1974).

26 Gahr, S. & Birnbaum, H. K. Hydrogen Embrittlement of Niobium .3. High-Temperature Behavior. *Acta Metall Mater* **26**, 1781-1788 (1978).

27 Shih, D. S., Robertson, I. M. & Birnbaum, H. K. Hydrogen Embrittlement of Alpha-Titanium - Insitu Tem Studies. *Acta Metall Mater* **36**, 111-124 (1988).

28 Dutton, R., Nuttall, K., Puls, M. P. & Simpson, L. A. Mechanisms of Hydrogen Induced Delayed Cracking in Hydride Forming Materials. *Metall Trans A* **8**, 1553-1562 (1977).

29 Li, J. C. M., Oriani, R. A. & Darken, L. S. Thermodynamics of Stressed Solids. *Z Phys Chem Neue Fol* **49**, 271-& (1966).

30 Flanagan, T. B., Mason, N. B. & Birnbaum, H. K. The Effect of Stress on Hydride Precipitation. *Scripta Metall Mater* **15**, 109-112 (1981).

31 Gahr, S., Grossbeck, M. L. & Birnbaum, H. K. Hydrogen Embrittlement of Nb .1. Macroscopic Behavior at Low-Temperatures. *Acta Metall Mater* **25**, 125-134 (1977).

32 Matsui, H., Kimura, H. & Moriya, S. Effect of Hydrogen on the Mechanical-Properties of High-Purity Iron .1. Softening and Hardening of High-Purity Iron by Hydrogen Charging during Tensile Deformation. *Mater Sci Eng* **40**, 207-216 (1979).

33 Moriya, S., Matsui, H. & Kimura, H. Effect of Hydrogen on the Mechanical-Properties of High-Purity Iron .2. Effect of Quenched-in Hydrogen Below Room-Temperature. *Mater Sci Eng* **40**, 217-225 (1979).

34 Matsui, H., Kimura, H. & Kimura, A. Effect of Hydrogen on the Mechanical-Properties of High-Purity Iron .3. Dependence of Softening on Specimen Size and Charging Current-Density. *Mater Sci Eng* **40**, 227-234 (1979).

35 Oriani, R. A. & Josephic, P. H. Effects of Hydrogen on the Plastic Properties of Medium-Carbon Steels. *Metall Trans A* **11**, 1809-1820 (1980).

36 Kimura, A. & Birnbaum, H. K. On the Kinetics of Intergranular Embrittlement of Nickel by Hydrogen Transport from the External Surface. *Scripta Metall Mater* **21**, 219-222 (1987).

37 Watson, J. W., Shen, Y. Z. & Meshii, M. Effect of Cathodic Charging on the Mechanical-Properties of Aluminum. *Metall Trans A* **19**, 2299-2304 (1988).

38 Kimura, A. & Birnbaum, H. K. Plastic Softening by Hydrogen Plasma Charging in Pure Iron. *Scripta Metall Mater* **21**, 53-57 (1987).

39 Sofronis, P. & Birnbaum, H. K. Mechanics of the Hydrogen-Dislocation-Impurity Interactions .1. Increasing Shear Modulus. *J Mech Phys Solids* **43**, 49-90 (1995).

40 Ferreira, P. J., Robertson, I. M. & Birnbaum, H. K. Hydrogen effects on the interaction between dislocations. *Acta Mater* **46**, 1749-1757 (1998).

41 Robertson, I. M. The effect of hydrogen on dislocation dynamics. *Eng Fract Mech* **68**, 671-692 (2001).

42 Robertson, I. M. & Birnbaum, H. K. An Hvem Study of Hydrogen Effects on the Deformation and Fracture of Nickel. *Acta Metall Mater* **34**, 353-366 (1986).

43 Tabata, T. & Birnbaum, H. K. Direct Observations of Hydrogen Enhanced Crack-Propagation in Iron. *Scripta Metall Mater* **18**, 231-236 (1984).

44 Bond, G. M., Robertson, I. M. & Birnbaum, H. K. The Influence of Hydrogen on Deformation and Fracture Processes in High-Strength Aluminum-Alloys. *Acta Metall Mater* **35**, 2289-2296 (1987).

45 Zapffe, C. A. & Sims, C. E. Hydrogen embrittlement, internal stress and defects in steel. *T Am I Min Met Eng* **145**, 225-261 (1941).

46 Symons, D. M. & Thompson, A. W. The effect of hydrogen on the fracture of alloy X-750. *Metall Mater Trans A* **27**, 101-110 (1996).

47 Oriani, R. A. & Josephic, P. H. Hydrogen-Enhanced Nucleation of Microcavities in Aisi-1045 Steel. *Scripta Metall Mater* **13**, 469-471 (1979).

48 Teter, D. F., Robertson, I. M. & Birnbaum, H. K. The effects of hydrogen on the deformation and fracture of beta-titanium. *Acta Mater.* **49**, 4313-4323 (2001).

49 Hirth, J. P. 1980 Institute of Metals Lecture the Metallurgical-Society-of-Aime - Effects of Hydrogen on the Properties of Iron and Steel. *Metall Trans A* **11**, 861-890 (1980).

50 Itsumi, Y. & Ellis, D. E. Electronic bonding characteristics of hydrogen in bcc iron .1. Interstitials. *J. Mater. Res.* **11**, 2206-2213 (1996).

51 Juan, A. & Hoffmann, R. Hydrogen on the Fe(110) surface and near bulk bcc Fe vacancies - A comparative bonding study. *Surf. Sci.* **421**, 1-16 (1999).

52 Irigoyen, B., Ferullo, R., Castellani, N. & Juan, A. The Location of a Hydrogen-Atom and Hydrogen Molecules in Bcc Fe - an Ased-Mo Approach. *Modell. Simul. Mater. Sci. Eng.* **3**, 319-329 (1995).

53 Pronsato, M. E., Pistonesi, C. & Juan, A. Density functional study of H-Fe vacancy interaction in bcc iron. *J Phys-Condens Mat* **16**, 6907-6916 (2004).

54 Tateyama, Y. & Ohno, T. Stability and clusterization of hydrogen-vacancy complexes in alpha-Fe: An ab initio study. *Phys Rev B* **67**, -, doi:Artn 174105

Doi 10.1103/Physrevb.67.174105 (2003).

55 Takai, K. & Shoda, H. Lattice Defect Formation and Degradation Enhanced by Hydrogen and Strain of Metals. *Effects of Hydrogen on Materials*, 195-202

765 (2009).

56 Farkas, D., Nogueira, R., Ruda, M. & Hyde, B. Atomistic simulations of the effects of segregated elements on grain-boundary fracture in body-centered-cubic Fe. *Metall Mater Trans A* **36A**, 2067-2072 (2005).

57 Itsumi, Y. & Ellis, D. E. Electronic bonding characteristics of hydrogen in bcc iron .2. Grain boundaries. *J. Mater. Res.* **11**, 2214-2219 (1996).

58 Liu, X. Y., Xie, W. B., Chen, W. X. & Zhang, H. Effects of grain boundary and boundary inclination on hydrogen diffusion in ♋-iron. *J. Mater. Res.* (2011).

59 Markworth, A. J. & Hirth, J. P. An Atomistic Model of Crack Extension by Kink Propagation. *J Mater Sci* **16**, 3405-3417 (1981).

60 Markworth, A. J. & Wolken, G. On the Calculation of Hydrogen-Metal Inter-Atomic Potentials. *Scripta Metall Mater* **15**, 1227-1230 (1981).

61 Mullins, M. Computer-Simulation of Fracture Using Long-Range Pair Potentials. *Acta Metall.* **32**, 381-388 (1984).

62 Decelis, B., Argon, A. S. & Yip, S. Molecular-Dynamics Simulation of Crack Tip Processes in Alpha-Iron and Copper. *J. Appl. Phys.* **54**, 4864-4878 (1983).

63 Hu, Z., Fukuyama, S., Yokogawa, K. & Okamoto, S. Hydrogen embrittlement of a single crystal of iron on a nanometre scale at a crack tip by molecular dynamics. *Modell. Simul. Mater. Sci. Eng.* **7**, 541-551 (1999).

64 Telitchev, I. Y. & Vinogradov, O. Numerical tensile tests of BCC iron crystal with various amounts of hydrogen near the crack tip. *Comp Mater Sci* **36**, 272-280, doi:DOI 10.1016/j.commatsci.2005.04.006 (2006).

65 Taketomi, S., Matsumoto, R. & Miyazaki, N. Atomistic study of the effect of hydrogen on dislocation emission from a mode II crack tip in alpha iron. *Int J Mech Sci* **52**, 334-338, doi:DOI 10.1016/j.ijmecsci.2009.09.042 (2010).

66 Matsumoto, R., Taketomi, S., Matsumoto, S. & Miyazaki, N. Atomistic simulations of hydrogen embrittlement. *Int. J. Hydrogen Energy* **34**, 9576-9584, doi:DOI 10.1016/j.ijhydene.2009.09.052 (2009).

67 Taketomi, S., Matsumoto, R. & Miyazaki, N. Atomistic study of hydrogen distribution and diffusion around a {112} < 111 > edge dislocation in alpha iron. *Acta Mater.* **56**, 3761-3769 (2008).

68 Matsumoto, R., Taketomi, S., Miyazaki, N. & Inoue, Y. Estimation of Hydrogen Distribution around Dislocations Based on First Principles Calculations. *Effects of Hydrogen on Materials*, 663-670

765 (2009).

69 Robertson, I. M. The effect of hydrogen on dislocation dynamics. *Eng Fract Mech* **64**, 649-673 (1999).

70 Atrens, A., Fiore, N. F. & Miura, K. Dislocation Damping and Hydrogen Pinning in Austenitic Stainless-Steels. *J. Appl. Phys.* **48**, 4247-4251 (1977).

71 Gavriljuk, V. G., Shivanyuk, V. N. & Foct, J. Diagnostic experimental results on the hydrogen embrittlement of austenitic steels. *Acta Materialia* **51**, 1293-1305, doi:Doi 10.1016/S1359-6454(02)00524-4 (2003).

72 Gavriljuk, V. G., Shivanyuk, V. N. & Shanina, B. D. Change in the electron structure caused by C, N and H atoms in iron and its effect on their interaction with dislocations. *Acta Mater* **53**, 5017-5024, doi:DOI 10.1016/j.actamat.2005.07.028 (2005).

73 Tiwari, G. P. *et al.* A study of internal hydrogen embrittlement of steels. *Mat Sci Eng a-Struct* **286**, 269-281 (2000).

74 Bernstei.Im. Effect of Hydrogen on Deformation of Iron. *Scripta Metall Mater* **8**, 343-350 (1974).

75 Asano, S. & Otsuka, R. Further Discussion on Lattice Hardening Due to Dissolved Hydrogen in Iron and Steel. *Scripta Metall Mater* **12**, 287-288 (1978).

76 Adair, A. M. Effect of Hydrogen Charging on Petch Relationship for Zone-Refined Iron. *Transactions of the Metallurgical Society of Aime* **236**, 1613-& (1966).

77 Kimura, H. & Matsui, H. Mechanism of Hydrogen-Induced Softening and Hardening in Iron. *Scripta Metall Mater* **21**, 319-324 (1987).

78 Asano, S. & Otsuka, R. Lattice Hardening Due to Dissolved Hydrogen in Iron and Steel. *Scripta Metall Mater* **10**, 1015-1020 (1976).

79 Lan, Y., Klaar, H. J. & Dahl, W. Effects of Hydrogen on Deformation-Behavior of Iron with Different Dislocation-Structures. *Scripta Metallurgica Et Materialia* **24**, 1659-1664 (1990).

80 Zhang, T. Y., Chu, W. Y. & Hsiao, C. M. Strain Field of Hydrogen in Alpha-Fe under Boltzmann Distribution. *Scripta Metall Mater* **19**, 271-274 (1985).

81 Zhang, T. Y., Chu, W. Y. & Hsiao, C. M. Strain Fields of Hydrogen-Atoms in Iron. *Scripta Metall Mater* **18**, 1421-1426 (1984).

82 Wen, M., Fukuyama, S. & Yokogawa, K. Atomistic simulations of effect of hydrogen on kink-pair energetics of screw dislocations in bcc iron. *Acta Mater* **51**, 1767-1773, doi:Doi 10.1016/S1359-6454(02)00575-X (2003).

83 Juan, A., Gesari, S., Brizuela, G. & Pronsato, M. E. A comparative study of the electronic structure of H pairs near a/2[1 (1)over-bar1] and a[010] dislocations in bcc Fe. *Appl. Surf. Sci.* **182**, 103-114 (2001).

84 Weber, U. *et al.* Influence of hydrogen on the deformation behaviour of a ferritic fine-grained low alloy steel. *Comp Mater Sci* **32**, 577-587, doi:DOI 10.1016/j.commatsci.2004.09.006 (2005).

85 Nedelcu, S. & Kizler, P. Molecular dynamics simulation of hydrogen-edge dislocation interaction in BCC iron. *Physica Status Solidi a-Applied Research* **193**, 26-34 (2002).

86 Takeuchi, T. Theory of Low Temperature Work-Hardening of Body-Centred Cubic Metals. *J. Phys. Soc. Jpn.* **27**, 436-& (1969).

87 Tang, M., Kubin, L. P. & Canova, G. R. Dislocation mobility and the mechanical response of BCC single crystals: A mesoscopic approach. *Acta Mater.* **46**, 3221-3235 (1998).

88 Louchet, F., Kubin, L. P. & Vesely, D. Insitu Deformation of Bcc Crystals at Low-Temperatures in a High-Voltage Electron-Microscope Dislocation Mechanisms and Strain-Rate Equation. *Philos Mag A* **39**, 433-454 (1979).

89 Kaufmann, H. J., Luft, A. & Schulze, D. Deformation Mechanism and Dislocation-Structure of High-Purity Molybdenum Single-Crystals at Low-Temperatures. *Cryst. Res. Technol.* **19**, 357-372 (1984).

90 Vitek, V. Computer-Simulation of Screw Dislocation-Motion in Bcc Metals under Effect of External Shear and Uniaxial Stresses. *P Roy Soc Lond a Mat* **352**, 109-124 (1976).

91 Takeuchi, T. Temperature Dependence of Work-Hardening Rat in Iron Single Crystals. *J. Phys. Soc. Jpn.* **26**, 354-& (1969).

92 Low, J. R. & Guard, R. W. The Dislocation Structure of Slip Bands in Iron. *Acta Metall.* **7**, 171-179 (1959).

93 Kumnick, A. J. & Johnson, H. H. Deep Trapping States for Hydrogen in Deformed Iron. *Acta Metall.* **28**, 33-39 (1980).

94 Devincre, B. & Roberts, S. G. Three-dimensional simulation of dislocation-crack interactions in BCC metals at the mesoscopic scale. *Acta Mater.* **44**, 2891-2900 (1996).

95 Haile, J. M. *Molecular dynamics simulation : elementary methods*. (Wiley, 1992).

96 Frenkel, D. & Smit, B. *Understanding molecular simulation : from algorithms to applications*. 2nd edn, (Academic Press, 2002).

97 Allen, M. P. & Tildesley, D. J. *Computer simulation of liquids*. (Clarendon Press ;

Oxford University Press, 1987).

98 Haile, J., Mansoori, GA,. Molecular - Based Study of Fluids. *Division of Industrial and Engineering Chemistry, American Chemical Society. Division of Physical Chemistry,American Chemical Society Meeting. Washington,D.C.American Chemical Society.* (1983).

99 Alder, B. J. & Wainwright, T. E. Phase Transition for a Hard Sphere System. *J Chem Phys* **27**, 1208-1209 (1957).

100 Gibson, J. B., Goland, A. N., Milgram, M. & Vineyard, G. H. Dynamics of Radiation Damage. *Phys Rev* **120**, 1229-1253 (1960).

101 Rahman, A. Correlations in Motion of Atoms in Liquid Argon. *Phys Rev a-Gen Phys* **136**, A405-& (1964).

102 Griebel, M. *Numerical simulation in molecular dynamics : numerics, algorithms, parallelization, applications*. 1st edn, (Springer Berlin Heidelberg, 2007).

103 Olander, D. R. Description of Hydrogen-Metal Interaction by a Morse Potential Function. *J. Phys. Chem. Solids* **32**, 2499-& (1971).

104 Foiles, S. M., Baskes, M. I. & Daw, M. S. Embedded-Atom-Method Functions for the Fcc Metals Cu, Ag, Au, Ni, Pd, Pt, and Their Alloys. *Phys Rev B* **33**, 7983-7991 (1986).

105 Ramasubramaniam, A., Itakura, M. & Carter, E. A. Interatomic potentials for hydrogen in alpha-iron based on density functional theory. *Phys Rev B* **79**, -, doi:Artn 174101

Doi 10.1103/Physrevb.79.174101 (2009).

106 Daw, M. S. & Baskes, M. I. Semiempirical, Quantum-Mechanical Calculation of Hydrogen Embrittlement in Metals. *Phys. Rev. Lett.* **50**, 1285-1288 (1983).

107 Mendelev, M. I. *et al.* Development of new interatomic potentials appropriate for crystalline and liquid iron. *Philos Mag* **83**, 3977-3994, doi:Doi 10.1080/14786430310001613264 (2003).

108 Ackland, G. J., Mendelev, M. I., Srolovitz, D. J., Han, S. & Barashev, A. V. Development of an interatomic potential for phosphorus impurities in alpha-iron. *J Phys-Condens Mat* **16**, S2629-S2642, doi:Doi 10.1088/0953-8984/16/27/003

Pii S0953-8984(04)72912-1 (2004).

109 Verlet, L. Computer Experiments on Classical Fluids .I. Thermodynamical Properties of Lennard-Jones Molecules. *Phys Rev* **159**, 98-& (1967).

110 Swope, W. C., Andersen, H. C., Berens, P. H. & Wilson, K. R. A Computer-Simulation Method for the Calculation of Equilibrium-Constants for the Formation of Physical Clusters of Molecules - Application to Small Water Clusters. *J. Chem. Phys.* **76**, 637-649 (1982).

111 Andersen, H. C. Molecular-Dynamics Simulations at Constant Pressure and-or Temperature. *J. Chem. Phys.* **72**, 2384-2393 (1980).

112 Andrea, T. A., Swope, W. C. & Andersen, H. C. The Role of Long Ranged Forces in Determining the Structure and Properties of Liquid Water. *J. Chem. Phys.* **79**, 4576-4584 (1983).

113 Nose, S. A Molecular-Dynamics Method for Simulations in the Canonical Ensemble. *Mol. Phys.* **52**, 255-268 (1984).

114 Hoover, W. G. Canonical Dynamics - Equilibrium Phase-Space Distributions. *Phys Rev A* **31**, 1695-1697 (1985).

115 Parrinello, M. & Rahman, A. Polymorphic Transitions in Single-Crystals - a New Molecular-Dynamics Method. *J. Appl. Phys.* **52**, 7182-7190 (1981).

116 Parrinello, M. & Rahman, A. Crystal-Structure and Pair Potentials - a Molecular-Dynamics Study. *Phys. Rev. Lett.* **45**, 1196-1199 (1980).

117 Born, M. & von Karman, T. On fluctuations in spatial grids. *Phys Z* **13**, 297-309 (1912).

118 Plimpton, S. Fast Parallel Algorithms for Short-Range Molecular-Dynamics. *J Comput Phys* **117**, 1-19 (1995).

119 Takaki, S. Limit of dislocation density and ultra-grain-refining on severe deformation in iron. *Thermec'2003, Pts 1-5* **426-4**, 215-222 (2003).

120 Natori, M., Futamura, Y., Tsuchiyama, T. & Takaki, S. Difference in recrystallization behavior between lath martensite and deformed ferrite in ultralow carbon steel. *Scripta Mater.* **53**, 603-608, doi:DOI 10.1016/j.scriptamat.2005.04.025 (2005).

121 Jiang, D. & Carter, E. Diffusion of interstitial hydrogen into and through bcc Fe from first principles. *Physical Review B* **70**, 064102, doi:10.1103/PhysRevB.70.064102 (2004).

122 Norskov, J. K. Covalent Effects in the Effective-Medium Theory of Chemical-Binding - Hydrogen Heats of Solution in the 3d-Metals. *Physical Review B* **26**, 2875-2885 (1982).

123 Companion, A. L., Liu, F. & Onwood, D. P. On the Location of a Hydrogen-Atom in Body-Centered Cubic 3d Transition-Metal Lattices. *J Less-Common Met* **107**, 131-138 (1985).

124 Minot, C. & Demangeat, C. The Iron Hydrogen System - Lattice Location of Hydrogen, Heat of Formation, and Hydrogen Hydrogen Binding-Energy. *J Chem Phys* **86**, 2161-2167 (1987).

125 Miwa, K. & Fukumoto, A. First-principles study on 3d transition-metal dihydrides. *Phys Rev B* **65**, -, doi:Artn 155114

Doi 10.1103/Physrevb.65.155114 (2002).

126 Fukai, Y. Site Preference of Interstitial Hydrogen in Metals. *Journal of the Less-Common Metals* **101**, 1-16 (1984).

127 Takai, K., Shoda, H., Suzuki, H. & Nagumo, M. Lattice defects dominating hydrogen-related failure of metals. *Acta Mater.* **56**, 5158-5167, doi:DOI 10.1016/j.actamat.2008.06.031 (2008).

128 Olmsted, D. L., Hector, L. G. & Curtin, W. A. Molecular dynamics study of solute strengthening in Al/Mg alloys. *J Mech Phys Solids* **54**, 1763-1788, doi:DOI 10.1016/j.jmps.2005.12.008 (2006).

129 Zhang, F. & Curtin, W. A. Atomistically informed solute drag in Al-Mg. *Modell. Simul. Mater. Sci. Eng.* **16**, -, doi:Artn 055006

Doi 10.1088/0965-0393/16/5/055006 (2008).

130 Yu, S., Wang, C. Y. & Yu, T. The kink-pair nucleation in edge dislocation motion. *Solid State Sci* **11**, 733-739, doi:DOI 10.1016/j.solidstatesciences.2008.08.005 (2009).

131 Abraham, D. P. & Altstetter, C. J. The Effect of Hydrogen on the Yield and Flow-Stress of an Austenitic Stainless-Steel. *Metall Mater Trans A* **26**, 2849-2858 (1995).

132 Wilcox, B. A. & Smith, G. C. Portevin-Le Chatelier Efect in Hydrogen Charged Nickel. *Acta Metall.* **12**, 371-& (1964).

133 Friedel, J. *Dislocations*. [1st English edn, (Pergamon Press; U.S.A. ed. distributed by Addison-Wesley Pub. Co., Reading, 1964).

134 Lindemann, F. A. The calculation of molecular natural frequencies. *Phys Z* **11**, 609-612 (1910).

135 Pistonesi, C., Garcia, A., Brizuela, G. & Juan, A. A computational study of H-Fe vacancy interaction. *J Phys D Appl Phys* **31**, 588-594 (1998).

136 Ulmer, D. G. & Altstetter, C. J. Hydrogen-Induced Strain Localization and Failure of Austenitic Stainless-Steels at High Hydrogen Concentrations. *Acta Metall Mater* **39**, 1237-1248 (1991).

137 Tobe, Y. & Tyson, W. R. Effect of Hydrogen on Yield of Iron. *Scripta Metall Mater* **11**, 849-852 (1977).